Defence Research and Development Canada
Recherche et développement pour la défense Canada

DEFENCE R&D DÉFENSE

Mock Urban Setting Trial: Data Analysis and Interpretation

Eugene Yee
Defence R&D Canada – Suffield

Technical Report
DRDC Suffield TR 2003-097
December 2003

Canada

Mock Urban Setting Trial: Data Analysis and Interpretation

Eugene Yee
Defence R&D Canada – Suffield

Defence R&D Canada – Suffield
Technical Report
DRDC Suffield TR 2003–097
December 2003

Author

Eugene Yee

Approved by

Dr J. Lavigne
Head, Chemical and Biological Defence Section

Approved for release by

Dr R. Clewley
Chair, DRDC Suffield DRP

Abstract

This report describes a comprehensive study of the statistical characteristics of concentration fluctuations in a neutrally buoyant tracer plume dispersing through a large array of building-like obstacles, each of which measured 12.2 m × 2.42 m × 2.54 m. The plumes were released both upwind and within the obstacle array for a range of source heights between 0.15 and 5.2 m. Detailed flow field and instantaneous plume concentration data were obtained from a comprehensive series of tracer experiments which utilized a large number of high-resolution concentration detectors. accompanied by the simultaneous acquisition of meteorological and turbulence measurements with sonic anemometer/thermometers. Extensive analyses are performed on the plume concentration data, and results are presented for a number of concentration statistics such as the mean plume lateral and vertical spreads, mean concentration, fluctuation intensity, peak concentration to concentration standard deviation ratio, concentration probability density function (pdf), concentration power spectra, and various concentration time and length scales of dominant motions in the array plume (e.g., integral scale, Taylor microscale).

For the range of downwind distances from the source examined, the lateral mean concentration profiles are well approximated by a Gaussian distribution. The vertical profiles of mean concentration develop in a rather complex manner with downwind distance, with the result that the reflected Gaussian form is generally a less than ideal description of the mean array plume in the vertical direction. A comparison of the array plume with an open-terrain plume as a function of downwind distance indicates that the obstacle array significantly increases the lateral and vertical plume spreads and decreases the magnitude of the plume centreline mean concentration. The small-scale, high-intensity turbulence generated in the obstacle array results in a drastic reduction in the concentration fluctuation level in the array plume compared to an open-terrain plume under similar conditions. The evolution of the concentration pdf at a fixed range, but with decreasing height from above and into the obstacle array is similar to that obtained at a fixed height but with increasing downwind distance from the source. The integral and Taylor microscale time and length scales of the plume increase significantly within the obstacle array. Concentration power spectra measured within the array had a greater proportion of the total concentration variance in the lower frequencies (energetic subrange), with a correspondingly smaller proportion in the higher frequencies (inertial-convective subrange). It is believed that these effects result from the rapid and efficient stirring and mixing of plume material by the small-scale, high-intensity turbulence within the array.

Résumé

Ce rapport décrit une étude approfondie des caractéristiques statistiques des fluctuations de la concentration, dans un panache traceur d'une densité de flottabilité neutre, se dispersant à travers un important réseau d'obstacles ressemblants à des bâtiments, chacun mesurant $12,2$ m $\times$ $2,42$m $\times$ $2,54$ m. Les panaches ont été dispersés contre le vent et à l'intérieur du réseau d'obstacles, à une hauteur variant de 0,15 à 5,2 m. Des champs de propagation détaillés et des données instantanées de concentrations de panaches ont été obtenus à partir de séries complètes d'essais à partir de traceurs utilisant un grand nombre de détecteurs de concentration de haute résolution. Ceci tout en effectuant l'acquisition simultanée de mesures météorologiques et des turbulences, au moyen d'anémomètres et thermomètres soniques. Des analyses extensives ont été effectuées sur les donnes de concentration du panache et les résultats sont présentés pour un certain nombre de statistiques de concentration telles que les écarts latéraux et verticaux du panache moyen, la concentration moyenne, l'intensité de la fluctuation, le rapport concentration maximale — écart-type de la concentration maximale, la fonction de densité de la concentration, les spectres de la puissance de la concentration ainsi que les échelles des durées et longueurs variées de concentration des motions dominantes, à l'intérieur du panache du réseau (par ex : l'échelle intégrale, l'échelle microscopique de Taylor).

En ce qui concerne la portée des distances, sous le vent à partir de la source, qui ont été examinées, les profils latéraux de la concentration moyenne sont bien estimés par une loi de Gauss. Les profils verticaux de concentration moyenne se développent d'une maniére assez complexe, dans la distance sous le vent, le résultat étant que la forme gaussienne qui est réfléchie forme une description du panache du réseau, dans le vertical, qui n'est pas idéale. Une comparaison du panache du réseau avec ceux qui se développent dans un champ libre en fonction de la distance sous le vent, indique que le réseau d'obstacles augmente de manière signifiante l'étendue du panache latéral et vertical et diminue l'ampleur de la concentration de la ligne médiane du panache. La turbulence, à petite échelle et de haute intensité, générée dans le réseau d'obstacles, résulte en une réduction drastique du niveau de fluctuation de la concentration dans le panache du rseau, compare celui en champ libre, dans des conditions similaires. L'évolution de la fonction de densité de la concentration à une distance donnée, mais d'une hauteur décroissante à partir du dessus et vers l'intérieur du réseau d'obstacles, est similaire à celle obtenue à une hauteur définie mais á une distance sous le vent croissante à partir de la source. Les échelles de durée et celles de longueur intégrales et à échelles microscopiques de Taylor du panache augmentent de maniére signifiante à l'intérieur du réseau d'obstacles. Les spectres de puissance de la concentration mesurés à l'intérieur du réseau avaient une proportion plus importante de la variance de la concentration totale

dans les fréquences plus faibles (sous intervalles d'énergie) avec une proportion plus petite correspondante dans les plus hautes fréquences (sous intervalles par inertie - de convection). On pense que ces effets résultent du brassage et du mélange des matières du panache causés par la turbulence, à faible échelle et de haute intensité, à l'intérieur du réseau.

Executive summary

Introduction: It is anticipated that Canadian Forces (CF) in the foreseeable future will have to fight in or protect urban areas, whether in battle, peace-making, peacekeeping, or counter-terrorist operations. The increased awareness and importance accorded by the public worldwide and their governments to maintain appropriate defences against chemical and biological warfare (CBW) agents in an urban (built-up) environment, the prediction of casualties and human performance degradation resulting from such releases, and the development of operational procedures and regulations to control, mitigate, and monitor the fate of CBW agents in urban areas with high population densities, will require mathematical modeling of urban wind flows and dispersion. One of the drawbacks in the computer simulation of urban flow and dispersion is the lack of experimental data. This capability gap impairs the development and thorough validation of numerical models. That difficulty has been partly addressed recently in the case of the design and implementation of the Mock Urban Setting Trial, for which extensive field measurements have been made available for the development and validation of urban flow and dispersion models.

Results: This report describes a comprehensive study of the statistical characteristics of concentration fluctuations in a neutrally buoyant tracer plume dispersing through a large array of building-like obstacles, each of which measured 12.2 m $\times$ 2.42 m $\times$ 2.54 m. The plumes were released both upwind and within the obstacle array for a range of source heights between 0.15 and 5.2 m. Detailed flow field and instantaneous plume concentration data were obtained from a comprehensive series of tracer experiments which utilized a large number of high-resolution concentration detectors, accompanied by the simultaneous acquisition of meteorological and turbulence measurements with sonic anemometer/thermometers. Extensive analyses are performed on the plume concentration data, and results are presented for a number of concentration statistics such as the mean plume lateral and vertical spreads, mean concentration, fluctuation intensity, peak concentration to concentration standard deviation ratio, concentration probability density function (pdf), concentration power spectra, and various concentration time and length scales of dominant motions in the array plume (e.g., integral scale, Taylor microscale).

For the range of downwind distances from the source examined, the lateral mean concentration profiles are well approximated by a Gaussian distribution. The vertical profiles of mean concentration develop in a rather complex manner with downwind distance, with the result that the reflected Gaussian form is generally a less than ideal description of the mean array plume in the vertical direction. A comparison of the array plume with an open-terrain plume as a function of downwind distance indicates that the obstacle array significantly

increases the lateral and vertical plume spreads and decreases the magnitude of the plume centreline mean concentration. The small-scale, high-intensity turbulence generated in the obstacle array results in a drastic reduction in the concentration fluctuation level in the array plume compared to an open-terrain plume under similar conditions. The evolution of the concentration pdf at a fixed range, but with decreasing height from above and into the obstacle array is similar to that obtained at a fixed height but with increasing downwind distance from the source. The integral and Taylor microscale time and length scales of the plume increase significantly within the obstacle array. Concentration power spectra measured within the array had a greater proportion of the total concentration variance in the lower frequencies (energetic subrange), with a correspondingly smaller proportion in the higher frequencies (inertial-convective subrange). It is believed that these effects result from the rapid and efficient stirring and mixing of plume material by the small-scale, high-intensity turbulence within the array.

Significance and Future Plans: The primary purpose of this report is to present a detailed picture of the concentration statistics in plumes from point sources dispersing through a large array of obstacles. The aim is to provide valuable basic data on the struc ture and development of array plumes that can be used to guide the construction and assessment of predictive models for dispersion in a built-up area.

Yee, E. 2003. Mock Urban Setting Trial: Data Analysis and Interpretation. DRDC Suffield TR 2003–097, Defence R&D Canada – Suffield.

Sommaire

Introduction: On prévoit que, dans un avenir assez rapproché, les Forces canadiennes (CF) devront combattre à l'intérieur des zones urbaines ou bien les défendre, soit au cours de batailles soit au cours d'opérations de maintien de la paix ou anti-terroristes. L'opinion publique et les gouvernements du monde entier, mieux avertis, accordent de plus en plus d'importance à la nécessité de maintenir un niveau approprié de défense, contre les agents de guerre chimiques et biologiques (CBW), dans les milieux urbains (bâtis). On prévoit aussi que le nombre de victimes, la dégradation des performances humaines résultant de telles émissions ainsi que la mise au point des procédures opérationnelles et des règlements d'exploitation mis en place pour contrôler, contenir et surveiller le devenir des agents de guerre CB dans les zones urbaines, ayant une population de haute densité, nécessitera une modélisation mathématique du mouvement des vents et celle de la dispersion d'un polluant atmosphérique. Un des inconvénients de la simulation par ordinateur des mouvements et de la dispersion en zone urbaine est le manque de données expérimentales. Cette lacune compromet la mise au point et la validation complète des modèles numériques. Cette difficulté a été partiellement résolue récemment dans le cas de la conception et de l'implémentation d'un Essai fictif en milieu urbain pour lequel ont été prises des mesures élaborées sur le terrain afin de réaliser la mise au point et la validation des modéles de mouvements et de dispersion en milieu urbain.

Résultats: Ce rapport décrit une étude approfondie des caractéristiques statistiques des fluctuations de la concentration, dans un panache traceur d'une densité de flottabilité neutre, se dispersant à travers un important réseau d'obstacles ressemblants à des bâtiments, chacun mesurant $12,2$ m $\times$ 2.42m $\times$ $2,54$ m. Les panaches ont été dispersés contre le vent et à l'intérieur du réseau d'obstacles, à une hauteur variant de 0,15 à 5,2 m. Des champs de propagation détaillés et des données instantanées de concentrations de panaches ont été obtenus à partir de séries complètes d'essais à partir de traceurs utilisant un grand nombre de détecteurs de concentration de haute résolution. Ceci tout en effectuant l'acquisition simultanée de mesures météorologiques et des turbulences, au moyen d'anémomètres et thermomètres soniques. Des analyses extensives ont t effectues sur les donnes de concentration du panache et les rsultats sont prsents pour un certain nombre de statistiques de concentration telles que les écarts latéraux et verticaux du panache moyen, la concentration moyenne, l'intensité de la fluctuation, le rapport concentration maximale — écart-type de la concentration maximale, la fonction de densité de la concentration, les spectres de la puissance de la concentration ainsi que les échelles des durées et longueurs variées de concentration des motions dominantes, à l'intérieur du panache du réseau (par ex : l'échelle intégrale, l'échelle microscopique de Taylor).

En ce qui concerne la portée des distances. sous le vent à partir de la source, qui ont été examinées. les profils latéraux de la concentration moyenne sont bien estimés par une loi de Gauss. Les profils verticaux de concentration moyenne se développent d'une maniére assez complexe. dans la distance sous le vent, le résultat étant que la forme gaussienne qui est réfléchie forme une description du panache du réseau, dans le vertical. qui n'est pas idéale. Une comparaison du panache du réseau avec ceux qui se développent dans un champ libre en fonction de la distance sous le vent, indique que le réseau d'obstacles augmente de manière signifiante l'étendue du panache latéral et vertical et diminue l'ampleur de la concentration de la ligne médiane du panache. La turbulence, petite échelle et de haute intensité, générée dans le réseau d'obstacles, résulte en une réduction drastique du niveau de fluctuation de la concentration dans le panache du rseau, compare celui en champ libre, dans des conditions similaires. L'évolution de la fonction de densité de la concentration à une distance donnée. mais d'une hauteur décroissante à partir du dessus et vers l'intérieur du réseau d'obstacles. est similaire à celle obtenue à une hauteur définie mais á une distance sous le vent croissante à partir de la source. Les échelles de durée et celles de longueur intégrales et à échelles microscopiques de Taylor du panache augmentent de maniére signifiante à l'intérieur du réseau d'obstacles. Les spectres de puissance de la concentration mesurés à l'intérieur du réseau avaient une proportion plus importante de la variance de la concentration totale dans les fréquences plus faibles (sous intervalles d'énergie) avec une proportion plus petite correspondante dans les plus hautes fréquences (sous intervalles par inertie - de convection). On pense que ces effets résultent du brassage et du mélange des matières du panache causés par la turbulence, à faible échelle et de haute intensité, à l'intérieur du réseau.

La portée des résultats et les plans futurs: Le but principal de ce rapport est de présenter en détails les statistiques de concentration dans les panaches, à partir de leur point d'origine de dispersion et à travers un important réseau d'obstacles. L'objectif est de fournir des donnes fondamentales précieuses au sujet de la structure et du développement du panache d'un réseau qui peuvent être utilisées comme guide dans la construction et l'évaluation de modèles de prdiction de la dispersion dans des zones bâties.

Table of contents

List of Figures

This page intentionally left blank

List of Tables

This page intentionally left blank

Acknowledgements

The Mock Urban Setting Trial (MUST) was sponsored by Defense Threat Reduction Agency (DTRA), and included participation from a number of government and academic laboratories in the United States, United Kingdom, and Canada. These included West Desert Test Center at U.S. Army Dugway Proving Ground, U.S. Department of Energy, U.S. Army Research Laboratory, University of Arizona, University of Utah, UK Defence Science and Technology Laboratory, and Defence R&D Canada – Suffield. The author would like to especially thank John Pace and James Bowers who provided the administrative and technical guidance on MUST. The technical support given by Geoff Chandler (Aurora Scientific Inc.) and Peter Kosteniuk (Kosteniuk Consulting Ltd) for their help in conducting the dispersion experiments is acknowledged. The significant contributions provided by Chris Biltoft on the successful implementation of MUST is gratefully acknowledged.

This page intentionally left blank

Introduction

In recent years, owing to an increasing likelihood of an accidental or deliberate release of a hazardous material in an urban (built-up) area such as an industrial complex or residential and commercial dense urban estate where the population density is high, considerable attention has focused on the development of models to predict the dispersion of toxic materials in the urban environment. Many studies of urban dispersion in the past have restricted attention to the far-field of the toxic release where the plume dimensions are significantly larger than the individual buildings. In this case, the enhanced dispersion arising from the (usually complicated) configuration of buildings in the urban complex is characterized simply as an increased surface roughness leading to a greater intensity of turbulence for plume dispersion (Martin [1]; Gifford and Hanna [2]). However, it is expected that the highest concentrations and the greatest potential for deleterious effects of exposure to the toxic material will occur in the near-field of the toxic release. In consequence, a number of researchers (e.g., Meroney [3] ; Hosker [4]; Hosker and Pendergrass [5]) have contributed to the important topic of the flow and near-field dispersion around a single building or a small group of buildings. Nevertheless, owing to its intrinsic complexity, the problem of near-field plume dispersion through large groups of obstacles has received attention only in recent years. In particular, the systematic investigations initiated by Baechlin et al. ([6], [7]), Jerram et al. [8], Davidson et al. ([9], [10]), and Macdonald et al. ([11], [12]) are notable and have contributed significantly to our current understanding of the behaviour of a passive neutrally-buoyant plume passing through a large array of obstacles. Hanna and Chang [13] describe the Kit Fox roughness obstacle field experiments conducted at the Frenchman Flat area of the Nevada Test Site in late August and early September, 1995. These experiments were designed to represent an oil refinery or chemical plant at approximately 1:10 scale, and included some ground-level dense gas releases with the initial cloud depth less than the obstacle height. In this study, the authors noted that the peak mean concentration in the cloud increased with increasing cloud advection speed, and observed that this relationship appeared to vary with the obstacle packing density which in turn dictated whether the increased turbulence intensity or decreased mean wind speed in the obstacle array produced the dominant effect.

Virtually all the research effort on the dispersion of plumes through groups of obstacles has focused exclusively on the description of the mean concentration field (the concentration field is described only in a time-averaged sense). The only notable exceptions to this are afforded by the study of Davidson et al. [9] who investigated the effect of an obstacle array on the structure of the plume from a continuous point source and by the investigation of

Pavageau and Schatzmann [14] who examined the statistical properties of the instantaneous concentration field produced by a continuous line source within a street canyon flow. The paucity of information concerning the statistical description of the concentration fluctuations of a plume as it passes through a large group of obstacles is a rather surprising state of affairs. Indeed, concentration fluctuations are a ubiquitous feature of dispersing plumes and, in recent years, it has been recognized that this feature has practical importance in a number of engineering and technological applications. Some examples include the probability of ignition of inflammable gases which depends upon the instantaneous concentration lying between the lower and upper flammability limits, irrespective of the mean concentration; the assessment of human health hazard from toxic substances where the response is nonlinear; and, estimation of the perception of odours which depends on whether instantaneous concentrations are likely to exceed certain critical threshold levels over short periods of time.

The importance of concentration fluctuations coupled with the recent availability of fast-response instrumentation for the measurement of the phenomenon has led to various experimental studies that have contributed significantly to the extensive body of knowledge that now exists concerning the statistical properties of concentration fluctuations in dispersing plumes. These studies have been mostly limited to dispersion over flat and relatively smooth terrain in order to minimize the complexities of the analysis and have included measurements made in wind tunnels and water channels (e.g., Fackrell and Robins [15]; Stapountzis et al. [16]; Bara et al. [17] as well as full-scale atmospheric measurements (e.g., Sawford et al. [18]; Dinar et al. [19]; Peterson et al. [20]; Mylne and Mason [21]; Mylne [22]; Yee et al. [23]; Yee et al. [24]. [25]; among others).

Because full-scale atmospheric studies of the detailed structure of fluctuating concentrations in a plume dispersing through a large array of building-like obstacles are rare, we have conducted a comprehensive series of tracer experiments with the goal of providing more extensive measurements of concentration fluctuation statistics in an array plume. The Mock Urban Setting Trial (MUST) described herein was designed to provide insight on the instantaneous dispersion of a tracer through a large array of building-like obstacles. The present study was motivated, in part, by a need to provide a better understanding of how the structure of a plume is modified as it disperses through a large array of obstacles and to subsequently identify the physical mechanisms responsible for this modification. With this in mind, mean concentration field characteristics and higher-order moment properties of the instantaneous plume concentration are measured at a large number of positions downwind of point sources located both upwind of and within an obstacle array for a number of different release heights. Even though the mean concentration field will be

studied, this paper is concerned primarily with the effects of a large group of obstacles on plume concentration fluctuations. as it is in this area that the main virtues of the work lie. It is believed that the present field experiment (viz.. MUST) is a logical addition to the series of previous experimental works on mean-field dispersion in array plumes and on the study of concentration fluctuations in open-terrain plumes.

This page intentionally left blank

Site, topography, and obstacle array

Site and topography

The measurements were carried out in September 2001 at Horizontal Grid on U.S. Army Dugway Proving Ground which is located in the Great Basin Desert of northwestern Utah, 40° 12.606′ N, 113° 10.635′ W. The site elevation is 1310 m above mean sea level. The test site is predominantly flat. The cross-sections in contour maps of the area surrounding the test site show that the terrain slopes gently upwards to the south with a slope of approximately 0.0005. Terrain features that may influence winds over Horizontal Grid include sand dunes 4 to 6 m in height located at about 1 km to the north. At about 12 km southeast of the site, Granite Mountain rises 700 m above the basin floor. Approximately 24 km northeast of the site is Cedar Mountain whose ridge rises 600 m above the basin floor.

During the experiments, the horizontally homogeneous site was covered with a mixture of sparse greasewood and sagebrush ranging in height from about 0.4 to 0.75 m. The average aerodynamic roughness length, z_0, and the displacement height, d, which were determined from mean wind profiles measured under near-neutral stratification (where the mean wind speed variation with height can be represented by a simplified semi-logarithmic relation) were 4.5 ± 0.5 cm and 0.37 ± 0.09 m, respectively. Both z_0 and d were not dependent on wind direction. The diagnosed value of d is somewhat uncertain, but appears consistent with the common rule of thumb that the displacement height should be chosen to be approximately three-quarters of the height of the roughness elements. The diagnosed value of z_0 appears to be relatively insensitive to the exact value of d.

Obstacle array

Each obstacle was a rectangular parallelepiped, with a width (W) of 12.2 m, length (L) of 2.42 m, and height (H) of 2.54 m. A total of 120 obstacles was placed in an aligned configuration consisting of 12 rows of 10 obstacles each with an average obstacle spacing of $\langle w \rangle = 7.9$ m in the spanwise (lateral, or y-) direction and $\langle l \rangle = 12.9$ m in the streamwise (or, x-) direction (see Figure 1). Consequently, the overall width and length of the obstacle array were 193 m and 171 m, respectively, giving a spanwise aspect ratio of width-to-height

(L_y/H) of 75.9 and a lengthwise aspect ratio of length-to-height (L_x/H) of 67.3 for the array. This gives a frontal area density (frontal area of obstacle $(W \times H)$ divided by the lot area per obstacle) of 0.10 and a plan area density (plan area of obstacle $(L \times W)$ divided by the lot area per obstacle) of 0.096 for the obstacle array. For ease of reference, each row and column of the obstacle array was assigned a letter from A through L and a number from 0 through 9, respectively (Figure 1). In this convention, the obstacle at the intersection of row X and column k will be denoted Xk where $X \in \{A, B, C, \ldots, L\}$ and $k \in \{0, 1, 2, \ldots, 9\}$.

The normal to the long face of the obstacles in the array was oriented 30° west of north to take advantage of the prevailing wind directions at the test site in the sector from SSW to SE, resulting in a flat and homogeneous upwind fetch of more than 10 km. The x (streamwise, or longitudinal) and y (spanwise, or transverse) coordinates are defined so that $x = 0$ is the front edge of the obstacle array and $y = 0$ is the midpoint (centreline) of the obstacle array. The z (vertical) coordinate is defined so that $z = 0$ is the ground surface beneath the obstacles. Consequently, with this coordinate system, the positive x-axis is directed 30° west of north, whereas the positive y-axis is directed 30° south of west. The unit vectors along the x-, y-, and z-axes form a right-handed coordinate frame. Furthermore, the following notation is used throughout this study: $u_1 = u$, $u_2 = v$, $u_3 = w$ are the instantaneous velocity components along the x-, y-, and z-directions, respectively; and, U_i and u_i' are the mean and turbulent fluctuations of the velocity, respectively, with $u_i = U_i + u_i'$ (hence, u_i' is the deviation of the total velocity u_i from its mean value U_i). In this paper, a primed variable will be used to denote a departure of that variable from its mean value.

Instrumentation and experimental details

Details of the instrumentation deployed and the experiments conducted in MUST are given in Biltoft [26]. so only a brief summary of the instrumentation used to acquire the data analysed here will be presented.

Mean velocity and turbulence measurements

Reliable measurements of the undisturbed, upwind flow that can be used to determine the state of the equilibrium surface-layer flow approaching the obstacle array is essential. Measurements of the vertical profiles of the mean horizontal wind velocity and turbulence in the upwind flow were obtained from a 16-m telescoping pneumatic mast erected 30.5 m ($12H$) upwind of the midpoint (centreline) of the front of the obstacle array. This mast was instrumented with three horizontal 2-dimensional (2-D) sonic anemometer/thermometers (Applied Technologies Inc., Model RSWS-211/2SX, 15 cm path length) at the 4-, 8-, and 16-m levels. Similarly, 2-D sonic anemometer/thermometers (Applied Technologies Inc., Model RSWS-211/2SX, 15 cm path length) were mounted at the 4-, 8-, and 16-m levels of a 16-m pneumatic mast deployed 30.5 m ($12H$) downwind of the back of the obstacle array. The sonic anemometer/thermometers were oriented 30° west of true north to take advantage of the prevailing winds within the SSW to SE sector.

Measurements of mean velocity and turbulence were obtained also within and above the obstacle array. Vertical profiles of mean wind speed and turbulence were obtained from the 32-m lattice tower located near the centre of the obstacle array (Figure 1). This tower was instrumented with four 3-dimensional (3-D) sonic anemometer/thermometers (Applied Technologies Inc., Model RSWS-211/3SX, 15 cm path length) at the 4-, 8-, 16-, and 32-m levels. Furthermore, four 6-m lattice-type towers were erected at or near the centre of the four quadrants of the array. These four towers (Figure 1), which were labeled as towers A (NW quadrant), B (SW quadrant), C (NE quadrant), and D (SE quadrant) were each instrumented with 3-axis Solent WindMaster ultrasonic anemometers (Gill Instruments Ltd) at the 2.4- and 6-m levels. Finally, four 3-D sonic anemometer/thermometers (Applied Technologies Inc., Model SATI/3VX, 15 cm path length) were deployed at a height of 1.15 m within a street canyon to study the pattern of the flow between two rows of obstacles. Three of these sonic anemometers were equally spaced in the streamwise direction across

the centre of the street canyon between obstacles $H6$ and $G6$ (Figure 1), whereas the fourth sonic anemometer was centred in the spanwise gap between obstacles $G6$ and $G7$. It should be pointed out that the probe (VX) of these sonic anemometers was designed primarily for turbulence measurements in canopies where the wind speed is low and the wind direction highly unpredictable. The Applied Technologies Inc. and Gill Windmaster sonic anemometer data were recorded at 10 Hz and 20 Hz, respectively.

Concentration measurements

In each experiment, propylene (C_3H_6) tracer gas was released at a point from a specially designed gas dissemination system that used a mass flow controller to maintain a constant flow rate. The gas dissemination system consisted of three propylene cylinders connected in parallel and immersed in a hot-water bath. A Matheson 1L-510 regulator was connected to the outlet of the cylinders to ensure a constant downstream pressure, and a flexible hose was used to connect the regulator to the inlet fitting of the mass flow controller (Teledyne Hastings-Raydist). This controller, which consisted of a sensor, electronic circuitry, a shunt, and a valve, was used to set, control, and measure the flow rate of gas through the dissemination system. The controller allowed a constant gas flow rate to be maintained at a user-selected reference level between 20 and 225 l min^{-1} to within about 2%. A quick-release connector mated the outlet fitting of the mass flow controller to the dissemination hose, which was connected to the base of the disseminator, a schedule 40 PVC (polyvinyl chloride) pipe 1 m in length and 0.05 m in diameter through which the gas was released.

The instantaneous plume concentrations were measured with two types of fast-response photo-ionization detectors: namely, digital photo-ionization (dPID) detectors manufactured commercially by Aurora Scientific Inc. (Aurora, Ontario, Canada) and Ultra Violet Ion Collector (UVIC) detectors made by Industrial Development Bangor Ltd (United Kingdom). These detectors draw a stream of air into a sampling volume that is exposed to a stream of ultra-violet (UV) radiation with a photon energy of about 10.6 eV, which is sufficient to ionize the tracer gas propylene. The ions produced are collected on an electrode system, the current being converted to a voltage signal which is digitized using a PC-controlled, high-speed, high-resolution 16-bit analog-to-digital (A-D) input-output board and multiplexer. Both types of detectors provide a frequency response of 50 Hz with a sensitivity of about 0.01 ppm by volume of propylene.

Horizontal profiles of concentration statistics were measured using 40 dPIDs which were

arrayed along four horizontal sampling lines that were parallel to and centred in the street canyons (Figure 1). Sampling lines 1, 2, 3, and 4 were centred in the street canyons between obstacle rows I and J, G and H, E and F, and C and D, respectively; and, these sampling lines consisted of 12, 9, 9, and 10 detectors, respectively. The concentration detectors along the four horizontal sampling lines were placed at a height, z_d, of 1.8 m ($z_d/H = 0.71$). Vertical profiles of concentration statistics were characterized by 8 dPIDs deployed on the 32-m lattice tower near the centre of the obstacle array at heights of 1, 2, 4, 6, 8, 10, 12, and 16 m and by 24 UVICs mounted on the four 6-m towers A, B, C, and D. On each of these 6-m towers, 6 UVICs were deployed at the following levels: 1, 2, 3, 4, 5, and 5.9 m.

In each experiment, the propylene gas was released and sampled continuously over a period of approximately 15 min. At the flow rates for the gas release (between 150 and 225 l min^{-1}), the negative buoyancy effects of the gas were insignificant (the release was passive). Time series of instantaneous concentrations were measured at various points in both horizontal and vertical cross-sections through the dispersing plume at various downwind distances from the source, and for five source heights ($z_s = 0.15$, 1.3, 1.8, 2.6, and 5.2 m; or, $z_s/H = 0.059$, 0.51, 0.71, 1.02, and 2.05). Measurements were made for sources positioned upwind of, within, and above the obstacle array. A total of 63 continuous source tracer release experiments were attempted. Twenty-one selected experiments were analyzed in detail. Pertinent tracer release parameters from these selected field experiments are summarized in Table 1. In Table 1, Q is the tracer release rate at the source, and (x_s, y_s, z_s) is the location of the source with respect to the coordinate system defined in Figure 1. The start time for each experiment refers to the time the gas tracer was first released from the source.

Data reduction

The velocity time series from the sonic anemometer/thermometers were examined for outliers and missing data points. Values of the instantaneous velocity that exceeded the limits of four standard deviations from the mean level were removed from the time series. The removed and missing data points were replaced using linear interpolation. However, outliers and missing data points in the velocity time series were rare (occurring less than about 0.0001% of the time). The corrected velocity time series from the sonic anemometer/thermometers were rotated in the horizontal plane to bring the u- and v-components of the velocity vector in alignment with horizontal axes aligned along the x- and y-directions (Figure 1) of the obstacle array. Linear trends were removed from these time series before calculation of relevant variances and covariances. This allowed, at each 3-D sonic anemome-

ter/thermometer probe, the measurement of eddy correlation stresses and heat fluxes, as well as the mean wind speed, mean wind direction, and temperature. The relative importance of shear and buoyancy to the turbulence production can be estimated through the Obukhov length (see Results).

Table 1. *Summary of tracer release data.*

Trial	Date	Start Time (MDT)	Q (l min^{-1})	(x_s, y_s, z_s) (m,m,m)
1	21-09-2001	01:04:00	175	(24.19, 10.05, 0.15)
2	21-09-2001	02:51:00	200	(24.19, −30.15, 0.15)
3	24-09-2001	18:52:00	200	(39.51, 90.45, 0.15)
4	24-09-2001	19:35:00	200	(39.51, 90.45, 1.8)
5	24-09-2001	20:34:00	200	(24.19, 50.25, 1.8)
6	24-09-2001	21:02:00	200	(24.19, 30.15, 0.15)
7	24-09-2001	21:51:00	200	(29.64, −30.15, 0.15)
8	24-09-2001	22:13:00	200	(29.64, −30.15, 1.8)
9	24-09-2001	22:35:00	200	(31.85, −30.15, 2.6)
10	24-09-2001	23:04:00	200	(8.87, 0.0, 1.8)
11	25-09-2001	18:30:00	225	(8.87, 70.35, 1.8)
12	25-09-2001	18:49:00	225	(8.87, 70.35, 0.15)
13	25-09-2001	21:51:00	225	(14.32, 70.35, 1.8)
14	25-09-2001	22:56:00	225	(29.64, 90.45, 0.15)
15	25-09-2001	23:21:00	225	(31.85, 90.45, 2.6)
16	25-09-2001	23:54:00	225	(31.85, 50.25, 5.2)
17	26-09-2001	20:55:00	225	(−24.0, −70.35, 1.3)
18	26-09-2001	21:32:00	225	(−1.0, −90.45, 1.3)
19	26-09-2001	21:58:00	225	(1.21, −90.34, 2.6)
20	26-09-2001	22:24:00	225	(−1.0, −70.35, 1.3)
21	26-09-2001	22:51:00	225	(−24.0, −70.35, 1.3)

The pre-processing of the concentration time series consisted of two basic steps: (1) drift correction to the baseline level of the concentration time series to remove any slow variations (trends) in the level over the sampling period; and, (2) conversion of the concentration time series (in A-D units) to absolute concentration (in ppm by volume) by application of the appropriate calibration curve (modelled as a second-degree polynomial) to the data. The baseline drift was removed by least-squares fitting cubic splines to the mean levels of the noise baseline segments (segments containing no rapid fluctuations of significantly non-zero concentration) in the concentration time series. The concentration detectors were calibrated

at regular intervals (throughout the experimental period) over their entire operating range using reference concentrations of 0. 5. 10.2, 50, 110, 200, and 400 ppm propylene in air. The second-order polynomial used to characterize the calibration curve was found to provide an accurate representation (to within ± 2 %) for the calibration data over the entire operating range of the detectors.

Almost all the experiments in this study were conducted in a slightly to very stably stratified atmospheric surface layer. For stable conditions, the crosswind velocity variance can increase substantially due to the decrease of the friction velocity and increase of the relative contributions from the mesoscale variations. This can result in larger scale two-dimensional motions (e.g., larger than the characteristic length or width of the obstacle array) that may persist for long periods in the stable boundary layer, and these motions can enhance the meandering motion of plumes (Hanna [27]; Etling [28]). Hence, for long sampling times, these larger two-dimensional motions will dominate the dispersion obscuring the effect of the obstacle array on the turbulent diffusion. Because the crosswind velocity variance is sensitive to the range of scales included in its determination, the measurement of plume spread under these conditions can be potentially very sensitive to the choice of sampling time.

For a sampling time of approximately 15 min used in our experiments, the plume meandering caused by the quasi-horizontal mesoscale eddies in the stable boundary layer resulted generally in a slow drift in direction of the plume across the horizontal sampling lines. This result is generally further exacerbated by the difficulties and complexities associated with unsteadiness, non-uniformity, and sensitivity of flows to terrain slope in the stable boundary layer. To remove the effects of this non-stationarity from the data, the concentration time series for each plume dispersion experiment were conditionally sampled based on a careful examination of the records of mean wind speed and direction provided by the 2-D sonic anemometers deployed on the upwind mast. These records of mean wind speed and direction were used to extract the 200 s period within each 15 min plume dispersion experiment that exhibited the least variation in the mean wind speed and direction. This conditional sampling of the velocity and concentration time series restricts the range of scales included in its determination, and also makes possible a meaningful comparison of our results with previous investigations, both for field and wind tunnel experiments (e.g., Macdonald et al. [12]).

Our experimental measurements correspond to near-field dispersion in the obstacle array, where the travel time T is generally much less than the finite duration τ ($\approx$ 15 min) of the release (i.e., $T \ll \tau$). In all the selected experiments, $T < T_s \ll \tau$ where $T_s = 200$ s

is the fixed sampling duration of the standard period exhibiting the least variation in the mean wind. For the short range of downwind distances covered in our experiments, we expect the effective variation in the turbulent velocity statistics that determine the plume dispersion to be dominated by the fluctuations at the point of release over the period of the duration T_s of sampling of the concentration field. owing to the fact that the Lagrangian correlation coefficient is expected to fall only slowly (Hay and Pasquill [29]). In other words, the magnitude of the scale of turbulence is expected to be irrelevant to the turbulent spread of contaminant material *close* to a continuous point source. However, the scale of the turbulence must become increasingly important to the determination of the plume spreading as the ratio of the time of travel to the Lagrangian time scale increases.

It seems reasonable that the turbulence statistics (e.g., velocity variances) that determine the plume dispersion over the range of limited downwind distances covered in our experiments will be those corresponding to the sampling period T_s of the plume concentration field, provided the time of travel T is not substantially larger than T_s. In addition, in some of the experiments (especially those conducted under near neutral or slightly stable stratification with the higher mean wind speeds). we found a remarkable steadiness in the statistical values of the standard deviation of velocity (e.g., in these experiments, we found that the crosswind velocity standard deviation sampled over 600 s was less than 15 % larger than that sampled over 200 s, implying only a very gradual increase in the velocity standard deviation with increasing sampling time).

Results

Velocity statistics upwind, within, and downwind of the array

A compendium of mean wind and turbulence statistics data for the sampling periods selected for each experiment is given in Table 2. Here, wind components are calculated in the rotated coordinate system with streamwise (u), spanwise (v), and vertical (w) components aligned with the x-, y- and z-directions, respectively (and their standard deviations are given by σ_u, σ_v, and σ_w, respectively). Measurements of the mean horizontal wind speed S_{04}, mean wind direction α, and standard deviation in the mean wind direction σ_α obtained from the 2-D sonic anemometer mounted at a height of 4 m on the upwind mast are summarized in Table 2. Here, $S \equiv \overline{(u^2+v^2)^{1/2}}$ is the horizontal wind speed where the overbar is used to denote a time averaged value, and $\alpha \equiv \overline{\tan^{-1}(v/u)}$ is the mean wind direction with a positive angle measured anti-clockwise from the horizontal x-axis (which is aligned along the direction normal to the front face of the array). Hence, $\alpha = 0°$ corresponds to a mean wind direction normal to the obstacle array. Measurements of turbulence obtained with the 3-D sonic anemometer/thermometer at the 4-m level on the 32-m vertical tower near the array centre are summarized also in Table 2. The turbulence kinetic energy (TKE), k, was estimated from

$$k = \frac{1}{2}(\sigma_u^2 + \sigma_v^2 + \sigma_w^2). \tag{1}$$

The Obukhov length, L_{MO}, was estimated as

$$L_{\mathrm{MO}} = -\frac{u_*^3 T}{\kappa g \overline{w'T'}}, \tag{2}$$

where u_* is the friction velocity, T is the mean sonic temperature, $\kappa \approx 0.4$ is the von Kármán constant for momentum diffusion, g is the acceleration due to gravity, and $\overline{w'T'}$ is the vertical temperature flux. The influence of the mean humidity flux on the value of L_{MO} was considered to be negligible. The friction velocity was estimated from

$$u_* = \left[\left(\overline{u'w'}\right)^2 + \left(\overline{v'w'}\right)^2\right]^{1/4}. \tag{3}$$

Finally, the mean rate of dissipation of turbulence kinetic energy, ϵ, was estimated from the measured u_* and L_{MO} using similarity theory modified for use in stable conditions as

$$\epsilon = \frac{u_*^3}{\kappa}\left(\frac{1}{z} + \frac{4}{L_{\mathrm{MO}}}\right). \tag{4}$$

Note that Eq. (4) was obtained from the TKE transport equation assuming local equilibrium whereby a balance exists between (shear and buoyant) production and dissipation of TKE ($u_*^2 \partial U/\partial z - u_*^3/(\kappa L_{\rm MO}) = \epsilon$, where U is mean wind speed), with the mean wind shear for stable conditions given by

$$\frac{\partial U}{\partial z} = \frac{u_*}{\kappa}\left(\frac{1}{z} + \beta\frac{1}{L_{\rm MO}}\right),$$

where $\beta \approx 5$ (Dyer [30]).

Table 2. *Summary of velocity statistics.*

Trial	S_{04} (ms^{-1})	α (deg)	σ_α (deg)	k ($\mathrm{m}^2\mathrm{s}^{-2}$)	u_* (ms^{-1})	$L_{\rm MO}$ (m)	ϵ ($\mathrm{m}^2\mathrm{s}^{-3}$)
1	2.35	17	5.7	0.359	0.26	91	0.013
2	2.01	30	7.3	0.306	0.25	62	0.013
3	3.06	−49	8.6	0.436	0.32	330	0.022
4	1.63	−48	4.0	0.148	0.08	5.8	0.0013
5	2.69	−26	1.8	0.251	0.17	4.8	0.012
6	1.89	−10	3.8	0.218	0.16	7.7	0.0073
7	2.30	36	9.8	0.409	0.35	150	0.030
8	2.68	30	7.9	0.428	0.35	150	0.030
9	2.32	36	8.2	0.387	0.26	48	0.014
10	2.56	17	6.2	0.367	0.25	74	0.012
11	7.93	−41	9.5	1.46	1.1	28000	0.80
12	7.26	−50	8.5	0.877	0.76	2500	0.28
13	3.89	−41	7.1	0.402	0.46	140	0.066
14	5.02	−42	9.2	0.877	0.66	240	0.19
15	4.55	−39	8.5	0.718	0.50	170	0.087
16	4.49	−47	7.9	0.727	0.44	120	0.059
17	3.34	39	8.3	0.362	0.36	170	0.032
18	4.00	39	7.6	0.582	0.42	220	0.048
19	2.98	43	9.1	0.505	0.39	130	0.042
20	2.63	26	9.5	0.484	0.35	120	0.030
21	3.38	36	7.8	0.537	0.37	130	0.036

Mean velocities and turbulence statistics were recorded by various sonic anemometers upwind, through, and downwind of the obstacle array. The sonic anemometer on the upwind mast at a height of 4 m was used to provide the reference mean horizontal wind speed S_{04} and turbulence kinetic energy k_{04} for normalizing the mean velocity and turbulence statistics, respectively, measured within and downwind of the obstacle array. Note that the subscript "04" is used here to denote a flow quantity that is measured in the undisturbed upwind flow at the 4-m level. Because the upwind 2-axis sonic anemometer at the 4-m level provided only the two horizontal components of the velocity, the reference turbulence kinetic energy k_{04} was estimated from the measurements of σ_u and σ_v, and an approximation that $\sigma_w \approx 0.4(\sigma_u^2 + \sigma_v^2)^{1/2}$. The estimate for σ_w was obtained from using the usual

turbulence scaling ratios typical of a neutrally stratified surface layer; namely, $\sigma_u/u_* = 2.5$, $\sigma_v/u_* = 2.0$, and $\sigma_w/u_* = 1.25$ (u_* is the friction velocity).

The spatial variation of the normalized mean horizontal wind speed S/S_{04} at various heights upwind, within, and downwind of the obstacle array is exhibited in Figure 2 for a mean wind direction nearly perpendicular ($|\alpha| = 10°$) and at a large flow incidence angle ($|\alpha| = 41°$) to the front face of the array. The reduction in the mean wind speed below or at canopy height is more significant for the near normally-incident flow than for the flow at an oblique incidence, although in both cases minimum wind speeds at or below the canopy top were observed after the third row. However, above the canopy height, the situation is reversed with the reduction in the mean wind speed being more pronounced for the 41° wind direction than for the near perpendicular wind direction. In addition, the mean wind shear observed near the canopy top in the array for a nearly perpendicular wind was larger than that observed for an oblique flow incidence.

Figure 3 shows the spatial variation of the normalized turbulence kinetic energy k/k_{04} with depth into the obstacle array at various heights for winds at near perpendicular and at an oblique flow incidence. The TKE increases at or near the canopy top as one progresses through the obstacle array. This is due to an intense shear layer at the top of the canopy, where the kinetic energy of the mean flow is converted into turbulence kinetic energy (shear production of TKE). In addition, the TKE generated upwind of a given fixed point in the array will be exported downwind by local advection and turbulent (and/or pressure) transport. We note that the increase in the TKE through the obstacle array (below, at, and just above the canopy top) is considerably greater for the case of near normal flow incidence than for that of an oblique flow incidence. The variation in the TKE below and above the canopy height is significantly greater for a near normal wind than for an oblique wind direction. Consequently, it would appear that the turbulence generated either by the obstacles themselves in the wake flow (wake production of TKE) or by the shear-generated turbulence produced near the canopy top in the inflected mean velocity profile is considerably greater for winds perpendicular to rather than at some oblique angle to the front of the obstacle array.

Figure 4 displays the variation of the bulk drag coefficient C_d ($\equiv u_*^2/S_4^2$) as a function of stability parameter L_{MO}^{-1}, using sonic anemometer data acquired at a height of 4 m on the 32-m vertical tower located near the array centre. For $L_{\mathrm{MO}}^{-1} \gtrsim 0.01$, the drag coefficient diminishes with increasing stability (decreasing L_{MO}). Note that the stability regime $L_{\mathrm{MO}}^{-1} \gtrsim 0.01$ corresponds to a very stable stratification where there is significant suppression of mechanical turbulence by the stable stratification (at 4-m height near the

array centre). As L_{MO}^{-1} increases within this range of values, the turbulence in the stable surface layer (overlying the obstacle array) becomes more intermittent and patchy, allowing the upper portions of the layer to decouple from the surface forcings. In particular, for $L_{\mathrm{MO}}^{-1} \gtrsim 0.01$ the drag coefficient exhibits a power-law decay with increasing stability ($C_d \sim (L_{\mathrm{MO}}^{-1})^{-r}$) where the power-law exponent is found to be $r \approx 1/2$ (± 10 %).

The mean wind speed profile, adjusted using the log-linear profile for stable conditions, can be written

$$S(z) = \frac{u_*}{\kappa}\left\{\ln\left(\frac{Z}{z_0}\right) + \beta\frac{Z}{L_{\mathrm{MO}}}\right\} \qquad \text{for } Z \gg z_0, \tag{5}$$

where $Z \equiv z - d$ is the displaced (effective) height, z_0 is the aerodynamic roughness length, d is the displacement height, and u_* is the surface friction velocity. The parameter β is usually taken to be 5, although published values can range from 3 to 9 (Businger et al. [31]; Dyer [30]; Högström [32]). Figure 4 shows the drag coefficient predicted using Equation (5) with $\beta = 5$ and the upwind roughness length and displacement height $z_0 = 0.045$ m and $d = 0.37$ m (see Site and Topography). Note that the value of the drag coefficient is underestimated using the upwind roughness length. This is because the air flow above the obstacle array produces an additional momentum flux, the form (pressure) drag, resulting in an increased friction velocity, as $\tau^{1/2} = (\tau^T + \tau^F)^{1/2}$, where τ is the total kinematic shear stress, τ^T is the turbulent kinematic shear stress, and τ^F is the additional kinematic shear stress arising from the form drag due to the presence of the obstacles. At a given height and wind speed and assuming that the mean wind profile above the obstacle array retains the form given in Equation (5), this implies an increased roughness parameter for the obstacle array (z_0 increases with increasing C_d). In particular, the bulk drag coefficient appears to be consistent with Equation (5) with $\beta = 5$ and an increased aerodynamic roughness length $z_0 = 0.20$ m. For the obstacle array, the displacement height is assumed to be 70% of the obstacle height H, so $d \approx 1.8$ m (reflecting an increased displacement of the flow over the obstacle array). The increased aerodynamic roughness length here simply reflects the two contributions to the total stress; namely, the turbulent surface friction (which can be described by the roughness length of the upwind fetch) and the pressure or form drag (which is produced by the obstacle array).

Mean concentration

Figure 5 displays typical crosswind profiles of the mean concentration C in the obstacle array at two downwind distances x_L from the source for near normal flow incidence (Trial

6). Here, x_L refers to the Euclidean distance in the horizontal x-y plane between the point source location and the position of the plume centreline along the horizontal sampling line. Also, in Figure 5, a spanwise coordinate Y referred to a survey line parallel to the lengthwise (or, along the x-direction) edge of the array and 4.76 m west of the obstacles in column 8 has been used; thus, $Y = y + 81.21$ m. The measurements suggest that the crosswind concentration profiles are well represented by a Gaussian distribution, a result that is consistent with the findings of Davidson et al. [9] and Macdonald et al. [11].

Vertical profiles of the mean concentration at the plume centreline are shown in Figure 6 for two different downwind distances and source release heights for array plumes from Trials 6 and 10. Depending on the location and height of the source and on the downwind distance from the source, the maximum mean concentration in a vertical plume cross-section can occur at the surface [Figure 6(a)] or above the surface [Figure 6(b)]. Hence, vertical profiles of mean concentration for plumes dispersing through an obstacle array develop in a rather complex manner in contrast to the simple Gaussian crosswind profiles.

To characterize the lateral and vertical growth of the mean plume, we fitted a Gaussian profile of the form

$$C(y) = C_{0y} \exp\left(-\frac{(y - y_c)^2}{2\sigma_y^2}\right), \tag{6}$$

to the lateral profiles of mean concentration and a reflected Gaussian model of the form

$$C(z) = C_{0z}\left\{\exp\left(-\frac{(z - z_c)^2}{2\sigma_z^2}\right) + \exp\left(-\frac{(z + z_c)^2}{2\sigma_z^2}\right)\right\}, \tag{7}$$

to the vertical profiles of mean concentration. Here, C_{0y} and C_{0z} are the lateral plume centreline mean concentration and vertical plume centreline mean concentration (neglecting reflection from the ground), respectively; σ_y and σ_z are the lateral and vertical plume standard deviations, respectively; and, y_c and z_c are the lateral displacement of the plume centroid and the plume height centroid, respectively. Figures 5 and 6 show typical examples of best-fit Gaussian and reflected Gaussian forms to the lateral and vertical mean concentration profiles, respectively. Although the Gaussian form provides very good agreement with the measured lateral mean concentration profiles, the reflected Gaussian form provides a less than ideal description of the vertical mean concentration profiles for many cases. In consequence, the derived vertical plume spread using the reflected Gaussian model, while useful for both modelling and practical purposes, is not as accurate as the derived lateral plume spread using the Gaussian model.

Releases within or just upwind (in the displacement zone just upwind of the front row) of the obstacle array can result in significantly different vertical mean concentration profiles

through the plume than releases well upwind of the array (well upwind of the zone where the flow is first influenced by the presence of the array). Figure 7 shows vertical profiles of the non-dimensional mean concentration K ($\equiv 10^{-6} C S_{04} H^2/Q$, where C is mean concentration in ppm (i.e., for pure undiluted gas $10^{-6}C = 1$), S_{04} is the upwind horizontal mean wind speed at 4 m, and Q is the tracer volume release rate in $m^3\ s^{-1}$) for these two release configurations. The Figure clearly illustrates the differences in the mean plume dispersion for these two situations (taken from Trials 17 and 18). Both releases were for a source set at a height of $H/2$ with the incident wind direction at $\alpha = 39°$. For releases well upwind of the front of the array, the mean flow streamlines are accelerated and deflected over the top of the array causing the plume centroid to be elevated and increasing the vertical growth of the plume. In contrast, for releases within or just upwind of the array, the downwash of the plume material around the obstacles arising from the diffusion of vorticity from the wakes of the obstacles results in an observed maximum mean concentration at ground level. The effective lifting of the plume centroid for sources located upwind of an obstacle array has previously been reported by Davidson et al. [9].

The presence of the obstacles results in a lateral deflection in the direction of the mean plume centreline relative to the mean wind direction in the approach flow. Figure 8, which shows the mean plume centreline angle θ (the angle between the positive x-direction and the vector from the source location to the location of the mean plume centreline) as a function of the mean wind direction α in the approach flow, illustrates this phenomenon. Note that for near-normal flow incidence with $|\alpha| \lesssim 20°$, the plume centreline direction is deflected towards the normal to the front face of the array ($|\theta| < |\alpha|$). This appears to be due to the wind deflection or channeling down the street canyons of the obstacle array aligned roughly along the SE-NW direction (i.e., more precisely the wind direction within the array should be around 30° from true north). However, for a greater obliquity of flow incidence, the mean plume centreline direction is deflected away from the normal to the front face of the array, implying the plume lateral displacement is due to the channeling of the wind along the street canyons of the array that are aligned approximately along the SW-NE direction (i.e., more precisely the wind direction within the array should be around 60 or 120° from true north). In summary then, the surface flow tends to be channeled approximately parallel to the street canyons roughly in the SE-NW direction when the wind above the obstacle array has a large component in this direction (when the approach flow is approximately normal to the front face of the array), but when the wind aloft of the array has a significant component away from this direction (when the approach flow is at an oblique angle greater than about 20° to the array front) then the wind in the array tends to be channeled approximately parallel to the street canyons roughly in the SW-NE direction (parallel to the front face of the array). This channeling of the surface wind in the obstacle array is reflected in the

observed behaviour of the lateral displacements in the mean centreline directions of the array plume.

The measured rates of lateral and vertical plume growth in the obstacle array for near perpendicular flow incidence are illustrated in Figure 9. Here, it should be noted that the vertical plume growth is represented by the vertical extent, $\sigma_{z,t}$ ($\sigma_{z,t} \equiv \left(\sigma_z^2 + z_c^2\right)^{1/2}$). To provide a reference for comparison, conventional results for lateral and vertical plume growth in open terrain obtained for various Pasquill-Gifford stability classes B, C, D, and E following Briggs (for a 10-minute sampling duration) are also included (Stern et al. [33]). Note that the lateral and vertical plume spreads as well as downwind distance from the source for the unobstructed plume (where the only scale factors are roughness length and boundary-layer height) have been normalized by H in order to allow a comparison to be made with the array plume results. At the short ranges considered here where the statistical theory (Csanady [34]) predicts that lateral and vertical plume spreads are proportional to downwind distance from the source, it is expected that the scaling of these plume parameters should be similar over a broad range of scales (providing a justification for the use of H as the scaling parameter for the unobstructed plume parameters).

The measurements of plume dispersion in the array shown in Figure 9 were conducted under moderately stable background atmospheric conditions (stability class E), so the lateral and vertical plume spreads for the array plume should be compared with the open-terrain Briggs dispersion curve for stability class E. This comparison shows that the lateral and vertical plume spreads of the array plume are both increased relative to that of the unobstructed plume dispersion under the same atmospheric stratification. At $x_L/H \approx 10$, the lateral plume spread is similar in magnitude to that in a plume dispersing in open terrain under stability class B and the subsequent rate of lateral plume growth in the array is similar to that of an open-terrain plume in stability class D. Similarly, the vertical plume spread through the obstacle array at $x_L/H \approx 15$ is similar to that of an open-terrain plume in stability class C, although the subsequent rate of growth is comparable to that for stability class E (viz., approximately the same as that for an unobstructed plume dispersing under the same background atmospheric stratification). Qualitatively similar results were obtained by Macdonald et al. [12] for increases in both the lateral and vertical plume widths for wide obstacles with aspect ratios W/H greater than unity. There, as here, it appears that for wide obstacles with $W/H > 1$ up to two-dimensional obstacles ($W/H \rightarrow \infty$), the lateral plume spread increased by a factor of 2–4 (at least near the source in the "inflationary phase" of plume growth).

A number of physical mechanisms are responsible for the observed rapid initial increase

(see Figure 9) in the lateral and vertical spreads of the array plume ("inflationary phase" of plume growth). The lateral divergence of streamlines around wide and low obstacles followed by entrainment and rapid mixing of the plume material across the width W of the obstacle in the wake region and/or the lateral plume displacement (and the concomitant increased lateral shear effect) increases the lateral plume spread. On the other hand, the rapid mixing of plume material in the obstacle wakes up to the height H of the obstacles and the vertical divergence of mean flow streamlines near the front of the array increases the vertical plume spread. In the case of a release upwind of the front face of the array, the upward drift (deflection) of the mean flow streamlines near the leading edge of the array results in an effective lifting of the plume centroid which enhances the upward vertical diffusion. In turn, plume material swept upwards to the obstacle height by the wake motions can sometimes be subsequently entrained into intermittent, large eddy structures that can rapidly transport the material upwards to a significant height. It is conceivable that these canopy-scale eddies dominate the vertical transport of momentum and scalar in a canopy. These large-scale eddy structures are the result of the inviscid instability to small perturbations arising from the inflected canopy mean velocity profile which sets the pattern for the coherent eddy generation at the canopy top. The characteristics of these coherent eddies have been studied by Raupach et al. [35] using the canopy-mixing layer analogy, and have been shown to scale with H rather than z.

The observed behaviour of the array plume growth rate can be explained as follows. The rate of spread of the plume in the lateral and vertical directions may be expressed in terms of the lateral (K_y) and vertical (K_z) turbulent diffusivities, respectively, as

$$\frac{d\sigma_y}{dx} = \frac{K_y}{S\sigma_y} \qquad \text{and} \qquad \frac{d\sigma_z}{dx} = \frac{K_z}{S\sigma_z}, \tag{8}$$

where $K_y \approx u_{\rm rms}\Lambda$ and $K_z \approx w_{\rm rms}\Lambda$ ($u_{\rm rms}$ and $w_{\rm rms}$ are characteristic velocities of the turbulence in the lateral and vertical directions, respectively; and, Λ is the turbulence integral length scale). The turbulence intensity ($u_{\rm rms}/S$ or $w_{\rm rms}/S$) is expected to be larger in the "urban" canopy than in open terrain due to the obstacle-generated turbulence. In order for the array plume growth rate to be comparable to that in an open-terrain plume, the increase of the turbulence intensity in the "urban" canopy relative to that in the open terrain (which increases the plume growth rate) must be compensated by the effects of the following two factors. Firstly, the scale of the turbulence in the canopy must be reduced relative to that in the open terrain. Secondly, the array plume spread (σ_y or σ_z) must be increased relative to the open-terrain plume spread. Both of these factors decrease the plume growth rate. In particular, the turbulence length scale in the canopy is comparable to the height of the obstacles, whereas the turbulence length scale in the open terrain (in

the incident flow) is generally much larger than typical building (obstacle) dimensions. For the obstacle array studied here, these three effects (increased turbulence intensity on the one hand, and decreased turbulence integral length scale and increased plume spreads on the other hand) compensate each other with the result that the rate of plume growth in the array after the initial rapid increase ("inflationary phase") is comparable to that in an open-terrain plume (at least over the range of x_L/H for which we have measurements). However, given that $d\sigma_y/dx \propto \sigma_y^{-1}$ [Equation (8)], it is conceivable that at very large downstream distance ($x_L/H \gg 1$) the lateral plume spread rate of the array plume could be actually smaller than that of the unobstructed plume (owing to the larger initial lateral array plume spread). This would imply that the lateral spread of the open-terrain plume would eventually "catch up" to that of the array plume, so that at this stage of plume development the open-terrain and array plumes would be comparable in "size".

Figure 10 exhibits the decay of the non-dimensional mean concentration at the plume centreline K_0 with downwind distance from the source through the obstacle array for different source heights and various directions θ of plume centreline dispersion through the array. The open terrain measurements of K_0 shown here were obtained by combining the results from a previous series of field experiments (Yee et al. [24]; Yee et al. [25]) conducted under near-neutral stability conditions. Note that this measured variation of K_0 in open terrain under near-neutral atmospheric stratification is generally consistent with the variation of the Pasquill-Gifford neutral (D) curve. However, the non-dimensional plume centreline mean concentration in the obstacle array (obtained under moderately to very stable stratification) falls nearer the stability class C curve rather than the class E curve. Hence, plume centreline mean concentrations are reduced considerably in the obstacle array relative to the open-terrain plume results. This effect for the wide obstacle array ($W/H \approx 4.8$) studied here is different than that obtained for an array of cubes ($W/H = 1$) where it was found that the plume centreline mean concentration in the array is similar to the open-terrain plumes (Davidson et al. [9]; Macdonald et al. [11]). It is evident that for the wide obstacle array considered here, the reduction in the mean wind speed within the array does not compensate for the significant increases in both the lateral and vertical plume widths (and significant increase in the plume area) and therefore the centreline mean concentration C_0 in the array plume is significantly smaller than the open-terrain plume under similar atmospheric conditions.

It is interesting to note that at downwind distances from the source greater than about $x_L/H \approx 30$, the rate of decrease of the centreline mean concentration in the array plume is less than that of an open-terrain plume dispersing under similar atmospheric conditions. This can be understood as follows. For simplicity, assume that the mean concentration field

can be approximated by a Gaussian distribution in both the lateral and vertical directions (i.e., neglect the surface reflection), with a centerline mean concentration given by $C_0 = Q_m/(2\pi S\sigma_y\sigma_z)$, where Q_m is the quantity of matter released per unit time (Stern et al. [33]). Consequently, the rate of decrease of C_0 with downwind distance x is

$$\frac{dC_0}{dx} = -C_0\sigma_y\sigma_z\left[\frac{1}{\sigma_z\sigma_y^2}\frac{d\sigma_y}{dx} + \frac{1}{\sigma_y\sigma_z^2}\frac{d\sigma_z}{dx}\right]. \tag{9}$$

Firstly, note that the total concentration flux $Q_m \propto C_0\sigma_y\sigma_z$ is a conserved quantity (more specifically, for a Gaussian mean concentration distribution with S constant, the total concentration flux through the vertical y-z plane is $Q_m = 2\pi SC_0\sigma_y\sigma_z$). For the obstacle array studied here, it was found that $d\sigma_y/dx$ and $d\sigma_z/dx$ (plume growth rates in the lateral and vertical directions) are comparable to an open-terrain plume dispersing under similar atmospheric conditions. Hence, on examination of the preceding equation, it is seen that the slow rate of decay of the centreline mean concentration in the array plume at the greater downwind distances from the source arises from the increased spreads of the array plume in both the lateral and vertical directions (due to the rapid initial plume growth in the "inflationary" phase of plume development).

Concentration fluctuation intensity

The parameter most frequently used to characterize concentration fluctuations is the fluctuation intensity, $i \equiv \sigma_\chi/C$, where $\sigma_\chi \equiv \left[\overline{(\chi - C)^2}\right]^{1/2}$ is the concentration standard deviation (χ denotes the instantaneous concentration). In order to consider the downwind development of the concentration fluctuations in an array plume in more detail, we focus attention on an example of concentration fluctuation profiles in the lateral and vertical directions obtained from the data in experiment number 6 where the approach flow was nearly perpendicular to the front of the obstacle array. Figure 11(a) displays the lateral profiles of i at various non-dimensional downwind distances x_L/H from the source, whereas Figure 11(b) exhibits a vertical profile of i along the mean plume centreline for this experiment. In Figure 11(a), the labels 1, 2, 3, and 4 refer to the sequence of four horizontal sampling lines in the experiment (Figure 1) with lines 1 and 4 located at the most southerly and most northerly positions, respectively, in the array.

The shapes of these profiles are similar to those obtained from plumes dispersing over open terrain (Mylne and Mason [21]; Mylne [22]; Yee et al. [24]; Yee et al. [25]). In particular,

the lateral cross-sections of fluctuation intensity are seen to increase towards the edges of the plume from a minimum at the plume centreline and exhibit an approximate bilateral symmetry about the mean plume centreline (implying that the mean wind direction was approximately perpendicular to the horizontal sampling lines of detectors). The vertical profile varies only slightly between $z/H = 0$ and 2 (within the roughness sublayer of the obstacle array), but increases rapidly higher up as the extreme upper edge of the plume is approached. Despite similarities in the general shapes of the lateral and vertical profiles of fluctuation intensity to those observed in open-terrain plumes, the curves of i here are nevertheless wider and flatter, another manifestation of the observed increase in the lateral and vertical mean plume spreads (Figure 9).

For the case of an open-terrain plume, $\sigma_\chi \approx C$ (the variation about the mean concentration is at least as large as the mean concentration itself) along the mean-plume centreline ($i_0 \gtrsim 1$). However, from Figure 11, it is seen that centreline values of i are considerably less than unity for plumes dispersing through an obstacle array. Hence, it appears that the decrease in the concentration standard deviation is much greater than even the reduction in the mean concentration in the array (Figure 10), implying a dramatic reduction in the strength of concentration fluctuations. Clearly, the change from an open-terrain plume to a plume dispersing in an obstacle array has a very large effect on i, reducing it by a factor of between 2 and 5 along the plume centreline, depending on x_L/H. Quantitatively similar results were obtained by Davidson et al. [9] for the centreline behaviour of i, where $i_0 = 1.6$ was reported for the control (open-terrain) plume in contrast to the significantly smaller value of $i_0 = 0.4$ for the array plume in an equivalent position.

A first qualitative explanation for the drastic reduction of i in the array plume is that the lateral and vertical meandering of the instantaneous plume in the obstacle array is reduced significantly in comparison to the open-terrain plume. The reduction in plume meander within the array can probably be attributed to two physical mechanisms: (1) the possible reduction in the scale of turbulence Λ between the obstacles to that of the obstacles ($\sim H$); and, (2) the observed increase in the lateral and vertical spreads of the plume (Figure 9). Hence, the dramatic increase in the ratio of the plume spread to the integral turbulence scale within the array relative to its value in open terrain would explain the reduced meandering of the array plume, and therefore a decrease in the value of i.

However, we note that the dramatic reduction in i for plumes within the array cannot arise solely from the reduction in the meandering contributions. Figure 12 compares the vertical profile of i measured within the obstacle array (Run 6) with a similar vertical profile of i measured at approximately the same downwind distance from the source in open terrain.

The data for the open-terrain plume were obtained from a previous experiment (Yee et al. [25]). In addition, the vertical profile of the conditional fluctuation intensity i_p for the open-terrain plume is also shown in Figure 12, with the subscript p used here to denote a conditional statistic which is determined from the non-zero concentrations only. Firstly, because the intermittency for the plume within the array is small (the concentration time series within the array plume appears as a continuous signal with practically no periods where the concentration was zero) $i \approx i_p$ within the mean-plume core of the array plume. Note that i for the array plume is less than i_p for the open-terrain plume (Figure 12) throughout most of the vertical extent of the plume. This implies that the significant reduction in i for the array plume is due not only to the reduction in the plume meander, but also to vigorous mixing of material internal to the plume, smoothing out the in-plume concentration fluctuations and transferring the concentration variance (energy) to smaller scales through the inertial-convective cascade. In summary, the decrease in the plume meander and increase in the dissipation of the concentration fluctuations for the array plume leads to the observed dramatic decrease in i.

The observed smoothing of the internal concentration fluctuations in the array plume can be understood as follows. Vorticity is generated at the various solid surfaces of the obstacles in the array through the no-slip condition. This vorticity is then transported throughout the fluid between the obstacles by convection and diffusion and also will be enhanced in the canopy flows via the mechanism of vortex-stretching. This results in the small-scale, high-intensity turbulence that is characteristic of the flow within the obstacle array. The fine-scale structure of the canopy turbulence has a significant effect on the instantaneous structure of the array plume. The concentration fluctuations in the array plume are smoothed by the vigorous stirring and mixing of the material by the fine-scale, high-intensity turbulence in the canopy, leading to a drastic reduction in the length scales as material volumes are thinned. In particular, the fine-scale random vortical structures in canopy turbulence of length scale $l \sim \sigma_i$ (σ_i is the mean instantaneous plume width) leads to the entrainment or engulfment of clean air parcels into the plume, followed by the stretching and folding of material interfaces (stirring) which generates internal concentration variance within the instantaneous plume. This straining of material volumes continues until length scales are reduced to where molecular diffusion becomes important. In the array plumes, this process of transferring the variance to smaller scales (inertial-convective subrange of plume motions) appears to be significantly accelerated, rapidly smoothing out the concentration fluctuations.

Figure 13 displays the decay of the plume centreline fluctuation intensity i_0 with normalized downstream distance x_L/H from the source for an open-terrain plume and for array plumes

with various centreline directions $|\theta|$ of dispersion through the array. Note that the array plumes exhibit significantly lower centreline fluctuation intensities for all plume centreline directions of dispersion in comparison with the open-terrain plume at any given x_L/H. However, the rate of decrease of i_0 in the array plumes for $x_L/H \gtrsim 30$ is comparable to the open-terrain plume. This rate of decrease is rather slow, and it is possible that i_0 asymptotically approaches a non-zero constant value, rather than decreases to zero. If the former case is correct, it appears that i_0 in the open-terrain plume reaches a near constant value of about 1.0 at long range, in contrast to the array plume where i_0 appears to asymptotically approach a near constant value of about 0.2 independent of the direction of plume centreline dispersion.

The downwind decay of centreline fluctuation intensity i_0 stratified by source height for a fixed plume centreline direction θ of dispersion (approximately or better) and by the mean plume centreline direction of dispersion are shown in Figures 14(a) and 14(b), respectively. We note that for sources above the "urban" canopy, the initial fluctuation intensity is larger than for sources inside the canopy. This is the result of the much stronger mixing processes within the canopy arising from the small-scale, high-intensity turbulence generated by the obstacles of the array. However, the initial decay rate of the plume fluctuation intensity for the source above the canopy top is greater than that for the source within the canopy, with the result that both the magnitude and rate of decay for both array plumes become comparable at greater downwind distances from the source (the initial source conditions are rapidly "forgotten" as the plume material is subject to the continued stirring and mixing processes within the canopy).

There appears to be a weak dependence of the fluctuation intensity level on the direction of plume centreline dispersion through the array, which in turn is a manifestation of the mean wind direction of the upstream flow (Figure 8). In particular, fluctuation intensity levels in the array plumes are larger when the mean wind direction is nearly perpendicular to the front of the array ($|\alpha| \approx 0°$) than when the mean wind direction is at some oblique angle. This may be due to the fact that when the wind direction is nearly perpendicular to the front face of the array, the obstacles are aligned with the wind; whereas, when the wind direction is at some oblique angle to the front face of the array, there are no longer channels through which the flow can pass and the array behaves more like a staggered array than an aligned array. The turbulent mixing of plume material appears to be more vigorous in the staggered array where the flow can impact onto neighboring obstacles than in the aligned array where the flow is aligned with the street canyons.

Concentration probability density function

The one-point probability density function (pdf) of concentration provides information on the distribution of instantaneous concentration measured at a fixed point in the plume. In particular, the concentration pdf summarizes all the one-point statistics of the plume fluctuations (e.g., all the concentration moments, the intermittency factor, peak-to-mean concentration ratio, etc.) and thereby clearly provides more complete statistical information than any of the individual fluctuation statistics presented above (e.g., mean concentration, fluctuation intensity).

Histograms of the instantaneous concentration χ normalized by the mean concentration C were compiled by sorting the concentration data into bins and appropriately normalizing the bin counts to form the concentration pdf $f(\chi/C)$. Figures 15 and 16 display the measured pdfs of χ/C along the mean plume centreline at various non-dimensional downwind distances x_L/H from the source and at various positions through a vertical plume cross-section at a fixed downwind distance, respectively. Experiment 13 was the source for these examples which were selected in order to illustrate the change in the shape of the pdf with downwind distance from the source and with height above the ground.

From Figure 15, it is seen that the concentration pdfs at the mean plume centreline at downwind distances of $x_L/H = 19.8$ and 30.7 (closer to the source) exhibit a bimodal form—broad peaks are observed at $\chi/C \approx 0.3$ and 1.2 (arguably, this pdf form might even be interpreted as being trimodal with the third broad peak at $\chi/C \approx 1.7$). Farther downwind from the source, these two peaks in the concentration pdf merge and the pdf assumes a unimodal form that becomes increasingly concentrated at $\chi/C \approx 1.0$ as the intermittency in the array plume tends to unity and the contaminant parcels in the plume become more and more well mixed. The lower and upper tails of the concentration pdf become shorter and shorter with increasing downwind distance from the source as the continued small-scale mixing in the array results in the homogenization of the in-plume structure.

Figure 16 documents the evolution of the concentration pdf with height z/H above the ground surface. Within the canopy, the pdf assumes a unimodal Gaussian-like form that is concentrated at $\chi/C \approx 1.0$ implying a "well-mixed" plume structure that results from the vigorous small-scale stirring and mixing of the canopy turbulence. Molecular diffusion enhanced by concentration-gradient straining (or, stretching and folding of material filaments) arising from the small-scale, high-intensity canopy turbulence produces a systematic reduction of the central concentration moments (e.g., mean concentration, concentration variance) and of the range of concentration values over which the pdf spans. Above the canopy, at

heights between about $z/H = 2.0$ and 3.5, the concentration pdf transitions to a bimodal form with a narrow sharp peak at $\chi/C \approx 1.3$, and a broader weaker peak at a lower non-zero concentration of $\chi/C \approx 0.3$. At still greater heights above the canopy (for $z/H \gtrsim 4.0$), the concentration pdf evolves from a bimodal form towards a unimodal form again, but now the unimodal form is exponential-like rather than Gaussian-like. In particular, the amplitude of the peak at $\chi/C \gtrsim 1.0$ decreases, while that at or near zero concentration increases. Because the intermittency effect is reflected in the probability of occurrence of zero or near zero concentrations, the increase in the zero or near zero concentration peak in the pdf simply implies that there is a higher probability of encountering clean ambient air parcels near the upper edge of the array plume (and, hence, a higher probability of observing concentrations close to zero).

Interestingly, a comparison of Figure 15 with Figure 16 shows that there is a remarkable resemblance between the evolution of the concentration pdf with increasing height above the ground (at a fixed downwind distance from the source) and that with decreasing downwind distance from the source (at the fixed height above the ground). The current experiments of dispersion in the obstacle array did not measure the concentration pdf in the very near-field region of the source (at a range of downwind distances within the first row or two of the obstacle array). It is interesting to consider whether the variation in the concentration pdf at shorter range would evolve into a unimodal exponential-like form in analogy with the evolution of the concentration pdf form at greater heights.

The transition in the concentration pdf, from the exponential-like unimodal form higher up in the plume above the array ($z/H \gtrsim 4$), to a bimodal form with broad peak concentrations at $\chi/C \approx 0$ and $\chi/C \approx 1$ in the height range between about $z/H = 2$ and 3.5, and finally to a Gaussian-like unimodal form with the peak at $\chi/C \approx 1$ for $z/H \leq 1$, implies a large change in the distribution of both low-amplitude events and high-amplitude bursts of plume concentration with height. In particular, the concentration pdfs measured within the obstacle array show shorter lower and upper tails than those measured further up in the plume above the array, implying that both very low and very high instantaneous concentrations (relative to C) are observed with a smaller frequency within the canopy. These features are consistent with the general appearance of the instantaneous concentration time series measured simultaneously in a vertical cross-section through the plume.

Figure 17 displays the ratio of the peak value of concentration χ_{99} to the concentration standard deviation σ_χ in a vertical cross-section at the mean plume centreline for experiment number 13. Here, the peak concentration χ_{99} is defined as the value which is exceeded only 1% of the time. Interestingly, χ_{99}/σ_χ is approximately constant over the plume cross-section

for heights above the roughness sublayer ($z/H \gtrsim 2$), but increases within the roughness sublayer above the canopy and into the canopy layer. In particular, above the roughness sublayer, the quantity χ_{99}/σ_χ assumes a nearly constant value of about 4.5, which is equal to the value obtained through the cross-section of an open-terrain plume (Fackrell and Robins [15]). However, within the canopy layer, χ_{99}/σ_χ increases to a value between about 6 and 7, implying that the reduction in the peak value of concentration is less than the concentration standard deviation here. This is manifested also in the shape of the concentration pdf—although the concentration pdfs measured within the canopy are Gaussian-like (Figure 16), an interesting characteristic of these distributions is their slight *asymmetry* in the sense that the upper tail of the distribution appears to be slightly elongated compared to the lower tail. This is probably the result of the rapid turbulent mixing of the plume material by the small-scale, high-intensity turbulence within the canopy which effectively removes whatever large-scale concentration gradients there are in the array plume, forming patches of near constant concentration which can conform with the existing large-scale gradients only by the formation of "fronts" (sheets of intense concentration gradient). This interpretation appears consistent with the appearance of the concentration time traces measured within the array, where "plateau and cliff" structures are evident.

It is useful to develop a mathematical model for the concentration pdf of the array plume. To this end, it is pragmatic to investigate pdf forms which can be fully specified, including the intermittency effect, using only two parameters. Three commonly used pdf models for the concentration which satisfy this constraint are the exponential pdf (Barry [36]), the clipped normal pdf (Lewellen and Sykes [37]), and the clipped gamma pdf (Yee and Chan [38]). The exponential pdf assumes the form

$$f(\chi) = \frac{\gamma^2}{C} \exp\left(-\frac{\gamma\chi}{C}\right) + (1-\gamma)\delta(\chi), \tag{10}$$

where γ is the intermittency factor, defined as the probability that the concentration is non-zero and $\delta(\cdot)$ is the Dirac delta function. The clipped normal pdf is given by

$$f(\chi) = \frac{1}{\sqrt{2\pi}\sigma_c} \exp\left(-\frac{(\chi-\mu_c)^2}{2\sigma_c^2}\right) + (1-\gamma)\delta(\chi), \tag{11}$$

where

$$\gamma = \gamma(\mu_c, \sigma_c) \equiv \frac{1}{2}\left(1 + \mathrm{erf}\left(\frac{\mu_c}{\sqrt{2}\sigma_c}\right)\right). \tag{12}$$

Here, μ_c and σ_c are location and scale parameters, respectively and $\mathrm{erf}(\cdot)$ is the error function. Unlike a Gaussian pdf, $\mu_c \neq C$ for the clipped normal pdf. Finally, the clipped gamma pdf is defined as

$$f(\chi) = \left(\frac{\chi+\lambda}{s}\right)^{k-1} \frac{\exp\left(-(\chi+\lambda)/s\right)}{s\Gamma(k)} + (1-\gamma)\delta(\chi), \tag{13}$$

where s, k, and λ are scale, shape, and shift parameters, respectively, that are constrained as follows:

$$\gamma \equiv \gamma(k, s, \lambda) = 3\left[\overline{(\chi/C)^2}\right]^{-1} = \frac{\Gamma(k; \lambda/s)}{\Gamma(k)}, \tag{14}$$

where $\overline{(\chi/C)^2}$ is the normalized mean-square concentration. Here, $\Gamma(x)$and $\Gamma(\nu; x)$ denote the Gamma function and incomplete Gamma function, respectively. We note that for the case where $\gamma \rightarrow 1^-$ [or, equivalently $i \equiv \left(\overline{(\chi/C)^2} + 1\right)^{1/2} \rightarrow \sqrt{2}$ in accordance to Equation (14)], $\lambda \rightarrow 0^+$, and the clipped gamma distribution reduces to the standard gamma distribution. Because $\gamma = 1$ is the upper bound for the intermittency factor, for cases where $i \leq \sqrt{2}$ the standard gamma distribution with parameters s and k is applied ($\lambda = 0$ here).

To determine how well the model pdfs represent the concentration data, it is useful to construct quantile-quantile (Q-Q) plots that compare the order statistics from the sample data with those from the model distributions. Recall that the quantile of order q ($0 < q < 1$), designated by χ_{100q}, is the unique solution of the equation $F(\chi_{100q}) \equiv \Pr(\chi \leq \chi_{100q}) = q$ (the concentration level, χ_{100q}, exceeds the instantaneous concentration values with probability q).

Figure 18 presents the Q-Q plots of the observed data quantiles against the predicted (model) quantiles for 2 of the 3 theoretical distributions summarized above. We note that the exponential distribution cannot be used to model the plume concentrations in the examples of Figure 18 because the observed fluctuation intensities were less than unity. The data are taken at various heights along the centreline of an array plume at a fixed downwind distance from the source (Trial 13). An exact fit between the observed and model distribution results in a straight line with slope 1 and intercept 0 when the abscissa (observed quantiles) and ordinate (model quantiles) have equal scales. In the interpretation of the Q-Q plots, one should keep in mind that departures of the measured quantiles from the straight line in the extreme lower and upper tails of the distribution may simply reflect a lack of statistical convergence (viz., inadequate statistical sampling) in these extreme tails. With this caveat, it appears that the clipped normal and clipped gamma distributions can represent adequately the observed concentration pdf over much of its entire range. Nevertheless, the clipped gamma distribution appears to be a better representation of the observed distribution than the clipped normal distribution. In particular, both the upper and lower tails of the observed distribution are better characterized by the clipped gamma distribution. The probability of non-zero concentrations, γ, is underpredicted by the clipped normal distribution with the consequence that the lower tail of the clipped normal pdf is generally lighter (shorter) than that for the observed concentration pdf. This tendency of the clipped normal

pdf to underpredict the lower tail of the concentration distribution has been noted earlier by Yee and Chan [38] for open-terrain plumes. Finally, the clipped gamma pdf appears to predict the slight asymmetry in the measured in-array concentration pdfs as well as the elongation of the observed upper tail better than the clipped normal pdf.

Concentration power spectra

The normalized power spectral density of concentration fluctuations, $nS_\chi(n)/\sigma_\chi^2$, plotted against frequency, n, are exhibited in Figure 19 for a number of different heights above the ground at the centreline of an array plume at a range of around $x_L/H = 30.7$ (experiment 13). Here, $S_\chi(n)$ is the concentration power spectral density. The concentration power spectral density was estimated by dividing the entire time series into a number of blocks, applying a Parzen window or taper to each block to suppress end effects due to finite truncation, computing the Fast Fourier Transform (FFT) of each block, and then averaging the squared modulus of the FFT (the raw periodogram) at each frequency over the different blocks to obtain an ensemble average estimate of the power spectral density at this frequency. The spectra in Figure 19 were measured on the 32-m tower near the centre of the obstacle array. The area under the various spectra in Figure 19 have been equalized by normalization by the variance of the concentration fluctuations in accordance to the relationship

$$\int_0^\infty S_\chi(n)\, dn = \sigma_\chi^2. \tag{15}$$

Hence, the concentration power spectra shown in Figure 19 are one-sided spectra.

For concentration spectra measured above the canopy top, there appears to be very little variation in the form of the spectra. All these spectra exhibit a pronounced peak at about 0.4 Hz, marking the beginning of an inertial-convective subrange. The establishment of small-scale motion in the plume concentration fluctuations is often connected with the existence of an inertial-convective subrange in which the slope of $\log(S_\chi(n))$ versus $\log(n)$ is $-5/3$ (Mylne and Mason [21]). The range of scales associated with the inertial-convective subrange corresponds to eddies on smaller scales than the instantaneous plume, and these eddy scales are responsible primarily for the internal mixing process which transfers fluctuation variance from large scale to the very small scales where it can be dissipated by molecular diffusion. It is seen that concentration spectra measured above the canopy exhibit a moderate frequency range in which the slope is of the order $-5/3$ (or, equivalently, $nS_\chi(n) \sim n^{-2/3}$) with the upper cutoff being at about 4 Hz. Hence, these spectra exhibit an inertial-convective subrange spanning about one decade in frequency between about 0.4 Hz and 4 Hz associated

with the range of scales at which concentration variance (energy) is transferred from large to small scales with negligible molecular dissipation and/or interaction with the gradients in the mean concentration field (i.e., gradient production). This range is associated with those frequencies that correspond to scales of motion that are small relative to the instantaneous plume width.

In contrast, the power spectra measured in the canopy layer ($z/H \leq 1$) are significantly different than those measured above the canopy top. In particular, a rapid drop-off in the concentration power spectra occurs in a narrow band of frequencies just greater than the spectral peak at about 0.4 Hz (i.e., 0.4 Hz $\lesssim n \lesssim$ 4 Hz) where the spectral slope is seen to be significantly more negative than $-5/3$. This drop-off in the spectral density is greater for positions that are deeper in the canopy (closer to the ground surface). In other words, there appears to be a monotonic reduction in spectral level for $n \gtrsim 0.4$ Hz with decreasing height above the ground within the urban canopy layer. At frequencies above about 4 Hz, all spectra (measured both within and above the urban canopy) are seen to drop-off rapidly with a logarithmic slope that is significantly more negative than $-5/3$.

The significant "loss" of spectral power at frequencies n slightly greater than the spectral peak at about 0.4 Hz for in-canopy concentration power spectra can be attributed to the enhanced small-scale stirring and mixing of plume material within the canopy. Indeed, the presence of the solid surfaces of the obstacles in the array leads to the generation of fine-scale turbulence or small-scale random vortical structures in the wake flows that act to mix the array plume elements internally, smoothing out the concentration fluctuations. This action is expected to result in a greater concentration variance loss from the high-frequency (small-scale) end, with the result that a greater fraction of the total variance of in-canopy concentration spectra is concentrated at the low frequency end compared with concentration spectra measured above the canopy. Hence, it appears that the fine-scale wake turbulence results in a rapid and efficient mixing of the plume material within the canopy layer, resulting in a short circuit of the eddy cascade of concentration variance (energy) through the inertial-convective subrange of scales.

Interestingly, the location of the spectral peak in the plots of $nS_\chi(n)$ versus $\log(n)$ does not appear to change as we descend into the "urban" canopy. This spectral peak in the array plume concentration fluctuations appears to remain invariant with increasing downwind distance from the source. In particular, the location of the concentration spectral peak n_p is at about 0.4 Hz; or, equivalently, $n_p H/S_H \approx 0.51 \pm 0.02$ (where S_H denotes the mean horizontal wind speed measured at the canopy top $z/H = 1$). This behaviour contrasts with the case of an open-terrain plume where it was generally found that the spectral

peak frequency shifts toward lower frequencies with increasing downwind distance from the source (Mylne and Mason [21]; Yee et al. [23]; Yee et al. [24]). In particular, for an open-terrain plume n_p is proportional to S/σ_y (Mylne and Mason [21]), where S is the mean horizontal wind speed and σ_y is the lateral plume spread, whereas in the array plume $n_p H/S_H \approx 0.51$. Hence, the spectral peak in the array plume concentration fluctuations appears to be imposed by the topological characteristics of the obstacle array, and appears to be related to the time scale H/S_H of turbulent eddies of the scale of the obstacles (wake scales). Furthermore, the time scale H/S_H is also comparable to the time it takes plume material entrained into the wake of an obstacle of height H to diffuse out of it (Vincent [39]). In summary then, the frequency of the spectral peak which does not change as we descend into the canopy can be interpreted as an inverse time scale for the energy-containing concentration eddies in the array plume, eddies that appear to be related to the wake scales of motion in the canopy.

Figure 20 shows an example of the cross-spectral density of array plume concentration fluctuations (which has been decomposed into the squared coherency $\kappa_{12}^2(n)$ and phase $\phi_{12}(n)$) between two points in the plume measured below the canopy height. The squared coherency $\kappa_{12}(n)$ between concentration time series $\chi_1(t)$ and $\chi_2(t)$ measured at $z = z_1$ and $z = z_2$, respectively, at frequency n is the squared modulus of the cross-spectral density $S_{12}(n)$ at n, normalized by the products of the two auto-spectral densities $S_1(n)$ and $S_2(n)$, so $\kappa_{12}(n) \equiv |S_{12}(n)|^2/(S_1(n)S_2(n))$. The phase $\phi_{12}(n)$ of $\chi_1(t)$ and $\chi_2(t)$ at frequency n is the argument (angle) of the cross-spectra density $S_{12}(n)$. Together, $\kappa_{12}^2(n)$ and $\phi_{12}(n)$ describe in the frequency domain the correlation structure between the concentration processes measured at $z/H = 0.4$ (point 1) and $z/H = 0.8$ (point 2). The phase spectrum $\phi_{12}(n)$ represents the "average value" of the phase shift between the components in $\chi(z/H = 0.4)$ and $\chi(z/H = 0.8)$ at frequency n (defined mod 2π) and is conventionally taken to be in the interval $(-\pi, \pi)$. However, the phase spectrum defined on the interval $(-\pi, \pi)$ exhibits discontinuities, and in order to avoid this complication, the phase spectrum displayed in Figure 20 has been phase "unwrapped" to provide a continuous function of n.

The squared coherency and phase spectra exhibited in Figure 20 show a sudden change from high-coherence, in-phase variations for $n \lesssim 0.4$ Hz to incoherent random fluctuations for $n > 0.4$ Hz. The correlation coefficient between the two concentration time series was 0.79 for this example (taken from Run 13) and can be seen to arise almost entirely from frequencies less than about 0.4 Hz (which coincides also with the concentration power spectral peak). The coherency in the plume concentration fluctuations measured at different heights in the canopy appear to be related to the wake scales of motion which extend to the top of the canopy (and are determined as such by the height H of the obstacles).

time scale variations must be the result of spatial variations in the plume itself. In particular, the increased time and length concentration scales within the canopy are consistent with the observation that the plume structure is smoother and less fragmented within the canopy as a consequence of the vigorous small-scale mixing imposed by the canopy turbulence. Finally, the integral and Taylor length scales at mid-canopy height are comparable to characteristic dimensions of the individual canopy elements—$\Lambda_\chi(z/H = 0.5) \approx L_F$ and $\Lambda_T(z/H = 0.5) \approx H$, where $L_F \equiv \sqrt{WH}$ is a characteristic dimension of the front face of the obstacle.

The Taylor time scale appears to be roughly constant over much of the vertical plume cross-section, with a moderate increase seen to occur only below the top of the canopy. The variations in the Taylor length scale seen in the height range $z/H \gtrsim 2$ are due solely to variations in the mean wind speed profile (i.e., the increase in the Taylor length scale with height above the canopy merely reflects the increase in the mean wind speed with height here).

The enhanced and rapid mixing of plume material in the obstacle array merges small-scale plume concentration structures, leading to a reduction in the frequency and number of low-amplitude events and high-amplitude bursts, which increases the concentration fluctuation integral and Taylor microscale time and length scales in the canopy. Hence, canopy turbulence in the obstacle array appears to function as an efficient "mixer", reducing the plume fluctuation intensity and increasing the plume time and length scales. In effect, the current measurements suggest that canopy turbulence acts as a truly effective mixing flow (flow that results in rapid mixing of material released into it). The rapid initial reduction in the plume fluctuation intensity within the obstacle array implies plume material filaments injected at any position in the "urban" canopy appear to be stretched (at least initially) at a geometrical or exponential rate, resulting in greatly enhanced concentration gradients (generated by the ever thinning and convoluted filaments) that facilitate rapid mixing by molecular diffusion. The increased time and length scales of plume concentration fluctuations in the canopy imply that the material distribution in the instantaneous plume is more coherent here. The coherent nature of the array plume has an important implication for plumes composed of inflammable material—in a coherent plume, there is a higher probability that an ignition source at a given position and time can result in complete burn-up because in this case, there is a greater chance that there is a continuous path of inflammable material extending back to the source.

This page intentionally left blank

Conclusions

The primary purpose of this paper is to present a detailed picture of the behaviour of concentration fluctuation statistics in plumes from point sources dispersing through a large array of obstacles. The aim is mainly to provide valuable basic data on the structure and development of array plumes that can be used to guide the construction and assessment of predictive models for dispersion in a built-up area. However, the basic field experiment conducted here has its own merit in that the effect of a large group of obstacles on the dispersion of a passive scalar can be investigated by analyzing the data presented herein. The main conclusions of this work may be summarized as follows.

(1) For plumes released from a small point source where the initial plume size is small relative to the size of the individual obstacles in the array, the lateral and vertical plume spreads are increased initially rather significantly (by a factor of 2 to 4) relative to an open-terrain plume measured under similar conditions ("inflationary phase" of array mean plume development). However, the rapid initial increase in the array plume dimensions is followed subsequently by a rate of growth that is approximately comparable to that of an open-terrain plume under the same atmospheric conditions. The observed initial increase in the lateral plume width was due to the large width-to-height ($W/H \approx 4.8$) aspect ratio of the obstacles used in this study.

(2) In the array of wide and low obstacles studied here, it was found that the mean plume centreline concentration in the array is generally significantly smaller (by a factor of 5 to 10) than that observed in an open-terrain plume under similar atmospheric conditions. This observation differs markedly from the case of an array of cubes (unity aspect ratio obstacles) where it was found that the centreline mean concentration (at the source height) was generally similar to or greater than that in the open-terrain plume (Davidson et al. [10]; Macdonald et al. [11]). Hence, for an array composed of obstacles with significant spanwise aspect ratio, it appears that the reduction in mean velocity within the array cannot counteract the significant increases in both the lateral and vertical plume spreads. In addition, we found that the rate of decay of the centreline mean concentration in the array plume at downwind distances $x_L/H \gtrsim 30$ was slower than that in an open-terrain plume dispersing under similar atmospheric conditions.

(3) Lateral profiles of the mean concentration are represented well with a Gaussian form. The crosswind mean concentration profiles in the array plume at different downwind distances from the source can well be collapsed onto a single Gaussian form when they are

normalized by the local peak mean concentration C_{0y} and the local lateral plume width σ_y. However, vertical profiles of the mean concentration develop in a rather complex manner with increasing downwind distance from the source, and generally it was found that the reflected Gaussian form is not always an ideal description of the vertical mean concentration distribution.

(4) The increased lateral and vertical plume spreads coupled with the reduction of the scale of turbulence in the obstacle array results in a significantly reduced plume meander. The reduction in plume meander and the smoothing out of the in-plume concentration fluctuations results in a drastic reduction in the fluctuation intensity of an array plume relative to an open-terrain plume under similar conditions. In particular, centreline fluctuation intensities in the array plume are generally a factor of between 2 and 5 smaller than those in the open-terrain plume depending on the downwind distance from the source. In addition, the initial rate of decay of concentration fluctuations is increased in the array plume in comparison with the open-terrain plume, although at greater downwind distances from the source ($x_L/H \gtrsim 30$) the rate of decay of concentration fluctuations in the array plume appears to be comparable to that in the open-terrain plume. The reduction in the fluctuation intensities is observed also in the array plume above the top of the "urban" canopy and is a direct consequence of the increased mean wind shear produced near the canopy height (e.g., near $z/H \approx 1$, $\partial S/\partial z \gg 1$), resulting initially in the rapid amplification of scalar gradients, followed by rapid molecular diffusion across the steep concentration gradients established by the increased shearing action.

(5) Rapid mixing of plume material results in the shortening of the lower and upper tails of the concentration pdf measured within the obstacle array, implying that both very low and very high concentrations are observed with smaller frequency here. The shortening of the lower tail in the concentration pdf is manifested in the increase in the intermittency factor γ (i.e., $\gamma \approx 1$) for plume concentration fluctuations in the "urban" canopy, implying there are significantly fewer pockets of clean (unmixed) air in the plume here. The pdf of the array plume concentrations obtained within the "urban" canopy rapidly develops a tendency towards a Gaussian-like form, albeit with a small asymmetry in the sense that the upper tail of the distribution is slightly longer than the lower tail. The rapid relaxation of the concentration pdf to a Gaussian-like form implies that $\tau_d \ll \tau_c$ (where τ_c and τ_d are the time scales characterizing the creation and destruction of plume concentration fluctuations), in turn implying a regime where molecular diffusion dominates. In this regime, a Gaussian pdf might be expected. Certainly, the concentration pdf forms observed are consistent with the notion of the importance of the continuous operation of fine-scale canopy turbulence in reducing gradients of plume concentration and promoting the blending of finely laminated

concentration patterns. Finally, we found that some simple two-parameter model distributions such as the clipped normal and clipped gamma pdfs were capable of modelling the distribution of scalar concentrations over a wide range of positions in the array plume.

(6) The concentration power spectra measured above the obstacle array exhibited a moderate inertial-convective subrange spanning about a decade in frequency. There was a dramatic reduction in the spectral power level in the inertial-convective subrange for the part of the plume lying within the obstacle array. Furthermore, the spectra here had more of the total concentration variance concentrated at the lower frequencies ($n \lesssim n_p \approx 0.4$ Hz). This suggests that the small-scale, high-intensity random motions in the canopy turbulence must be relatively more effective at smearing out concentration fluctuations at the small scales characteristic of the inertial-convective subrange (associated with the internal structure or patchiness in the plume) than they are at the larger scales characteristic of the energetic subrange.

This page intentionally left blank

References

1. Martin, D. O. (1971). An Urban Diffusion Model for Estimating Long-Term Average Values of Air Quality. *J. Air Pollut. Control Assoc.*, 21, 16–19.

2. Gifford, F. A. and Hanna, S. R. (1973). Modelling Urban Air Pollution. *Atmos. Environ.*, 7, 131–136.

3. Meroney, R. N. (1982). Turbulence Diffusion Near Buildings. E. J. Plate (ed.), *Engineering Meteorology*, Elsevier, Amsterdam, 481–525.

4. Hosker, R. P. (1984). Flow and Diffusion Near Obstacles. D. Randerson (ed.), *Atmospheric Science and Power Production*, Technical Information Center, U.S. Department of Energy, Washington, D.C., 241–326.

5. Hosker, R. P. and Pendergrass, W. R. (1987). *Flow and Dispersion Near Clusters of Buildings*, NOAA Technical Memorandum ERL ARL-153, Air Resources Laboratory, Silver Spring, Maryland.

6. Baechlin, W., Theurer, W., and Plate, E. J. (1991). Wind Field and Dispersion in a Built-up Area—A Comparison Between Field Experiments and Wind Tunnel Data. *Atmos. Environ.*, 25A, 1135–1142.

7. Baechlin, W., Theurer, W., and Plate, E. J. (1992). Dispersion of Gases Released Near the Ground in Built Up Areas: Experimental Results Compared to Simple Numerical Modelling. *J. Wind Eng. Ind. Aero.*, 41–44, 2721–2732.

8. Jerram, N., Perkins, R. J., Fung, J. C. H., Davidson, M. J., Belcher, S. E., and Hunt, J. C. R. (1995). Atmospheric Flow Through Groups of Buildings and Dispersion From Localized Sources. J. F. Cermak (ed.), *Wind Climate in Cities*, Kluwer Academic Publishers, Amsterdam, 109–130.

9. Davidson, M. J., Mylne, K. R., Jones, C. D., Phillips, J. C., Perkins, R. J., Fung, J. C. H., and Hunt, J. C. R. (1995). Plume Dispersion Through Large Groups of Obstacles: A Field Investigation. *Atmos. Environ.*, 29, 3245–3256.

10. Davidson, M. J., Snyder, W. H., Lawson, R. E., and Hunt, J. C. R. (1996). Wind Tunnel Simulations of Plume Dispersion Through Groups of Obstacles. *Atmos. Environ.*, 30, 3715–3731.

11. Macdonald, R. W., Griffiths, R. F., and Cheah, S. C. (1997). Field Experiments of Dispersion Through Regular Arrays of Cubic Structures. *Atmos. Environ.*, 31, 783–795.

12. Macdonald, R. W., Griffiths, R. F., and Hall, D. J. (1998). A Comparison of Results from Scaled Field and Wind Tunnel modelling of Dispersion in Arrays of Obstacles. *Atmos. Environ.*, 32, 3845–3865.

13. Hanna, S. R. and Chang, J. (2001). Use of the Kit Fox Field Data to Analyze Dense Gas Dispersion Issues. *Atmos. Environ.*, 35, 2231–2242.

14. Pavageau, M. and Schatzmann, M. (1999). Wind Tunnel Measurements of Concentration Fluctuations in an Urban Street Canyon. *Atmos. Environ.*, 33, 3961–3971.

15. Fackrell, J. E. and Robins, A. G. (1982). Concentration Fluctuations and Fluxes in Plumes from Point Sources in a Turbulent Boundary Layer. *J. Fluid Mech.*, 117, 1–26.

16. Stapountzis, H., Sawford, B. L., Hunt, J. C. R., and Britter, R. E. (1986). 'Structure of the Temperature Field Downwind of a Line Source in Grid Turbulence. *J. Fluid Mech.*, 165, 401–424.

17. Bara, B. M., Wilson, D. J., and Zelt, B. W. (1992). Concentration Fluctuation Profiles from a Water Channel Simulation of a Ground-Level Release. *Atmos. Environ.*, 26A, 1053–1062.

18. Sawford, B. L., Frost, C. C., and Allan, T. C. (1985). Atmospheric Boundary-Layer Measurements of Concentration Statistics from Isolated and Multiple Sources. *Boundary-Layer Meteorol.*, 31, 249–268.

19. Dinar, N., Kaplan, H., and Kleiman, M. (1988). Characterization of Concentration Fluctuations of a Surface Plume in a Neutral Boundary Layer. *Boundary-Layer Meteorol.*, 45, 157–175.

20. Peterson, H., Lamb, B., and Stock, D. (1990). Interpretation of Measured Tracer Concentration Fluctuations Using a Sinusoidal Meandering Plume Model, *J. Appl. Meteorol.*, 29, 1284–1299.

21. Mylne, K. R. and Mason, P. J. (1991). Concentration Fluctuation Measurements in a Dispersing Plume at a Range of up to 1000 m. *Quart. J. Roy. Meteorol. Soc.*, 117, 177–206.

22. Mylne, K. R. (1993). The Vertical Profile of Concentration Fluctuations in Near Surface Plumes. *Boundary-Layer Meteorol.*, 65, 111–136.

23. Yee, E., Kosteniuk, P. R., Chandler, G. M., Biltoft, C. A., and Bowers, J. F. (1993). Statistical Characteristics of Concentration Fluctuations in Dispersing Plumes in the Atmospheric Surface Layer. *Boundary-Layer Meteorol.*, 65, 69–109.

24. Yee, E., Chan, R., Kosteniuk, P. R., Chandler, G. M., Biltoft, C. A., and Bowers, J. F. (1994). Experimental Measurements of Concentration Fluctuations and Scales in a

Dispersing Plume in the Atmospheric Surface Layer Obtained Using a Very Fast Response Concentration Detector. *J. Appl. Meteorol.*, 33, 996–1016.

25. Yee, E., Chan, R., Kosteniuk, P. R., Chandler, G. M., Biltoft, C. A., and Bowers, J. F. (1995). The Vertical Structure of Concentration Fluctuation Statistics in Plumes Dispersing in the Atmospheric Surface Layer. *Boundary-Layer Meteorol.*, 76, 41–67.

26. Biltoft, C. A. (2001). Customer Report for Mock Urban Setting Test. DPG Document No. WDTC-FR-01-121, West Desert Test Center, U.S. Army Dugway Proving Ground, Dugway, Utah,

27. Hanna, S. R. (1983). Lateral Turbulence Intensity and Plume Meandering during Stable Conditions. *J. Clim. Appl. Meteorol.*, 22, 1424–1430.

28. Etling, D (1990). On Plume Meandering under Stable Stratification. *Atmos. Environ.*, 24A, 1979–1984.

29. Hay, J. S. and Pasquill, F. (1959). Diffusion from a Continuous Source in Relation to the Spectrum and Scales of Turbulence. *Adv. Geophys.*, 6, 345–365.

30. Dyer, A. J. (1974). A Review of Flux-Profile Relationships. *Boundary-Layer Meteorol.*, 7, 363–372.

31. Businger, J. A., Wyngaard, J. C., Izumi, Y., and Bradley, E. F. (1971). Flux-Profile Relationships in the Atmospheric Surface Layer. *J. Atmos. Sci.*, 28, 181–189.

32. Högström, U. (1988). Non-dimensional Wind and Temperature Profiles in the Atmospheric Surface Layer. *Boundary-Layer Meteorol.*, 42, 55–78.

33. Stern, A. C., Boubel, R. W., Turner, D. B., and Fox, D. L. (1984). *Fundamentals of Air Pollution (Second Edition)*, Academic Press Inc., San Diego, California.

34. Csanady, G. T. (1973). *Turbulent Diffusion in the Environment*, D. Reidel Publishing Company, Dordrecht, Holland.

35. Raupach, M. R., Finnigan, J. J., and Brunet, Y. (1996). Coherent Eddies and Turbulence in Vegetation Canopies: The Mixing Layer Analogy. *Boundary-Layer Meteorol.*, 78, 351–382.

36. Barry, P. J. (1977). Stochastic Properties of Atmospheric Diffusivity. *Sulphur and its Inorganic Derivatives in the Canadian Environment*, National Research Council of Canada, 313–358.

37. Lewellen, W. S. and Sykes, R. I. (1986). Analysis of Concentration Fluctuations from Lidar Observations of Atmospheric Plumes. *J. Climate Appl. Meteorol.*, 25, 1145–1154.

38. Yee, E. and Chan. R. (1997). A Simple Model for the Probability Density Function of Concentration Fluctuations in Atmospheric Plumes. *Atmos. Environ.*, 31, 991–1002.

39. Vincent, J. H. (1978). Scalar Transport in the Near Aerodynamic Wakes of Surface Mounted Cubes. *Atmos. Environ.*, 12, 1319–1322.

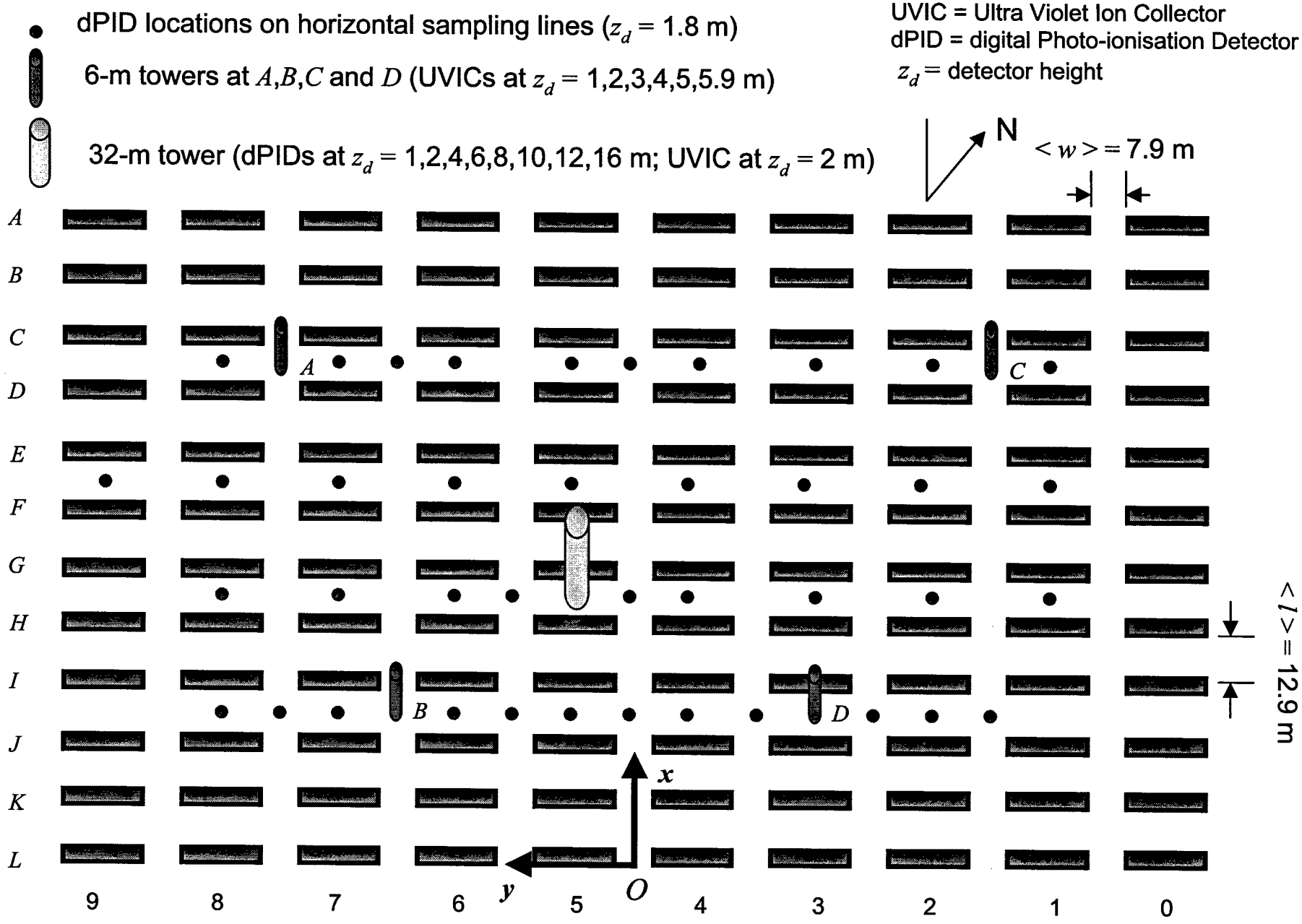

Figure 1. *A schematic diagram of the geometry of the Mock Urban Setting Trial (MUST) obstacle array.*

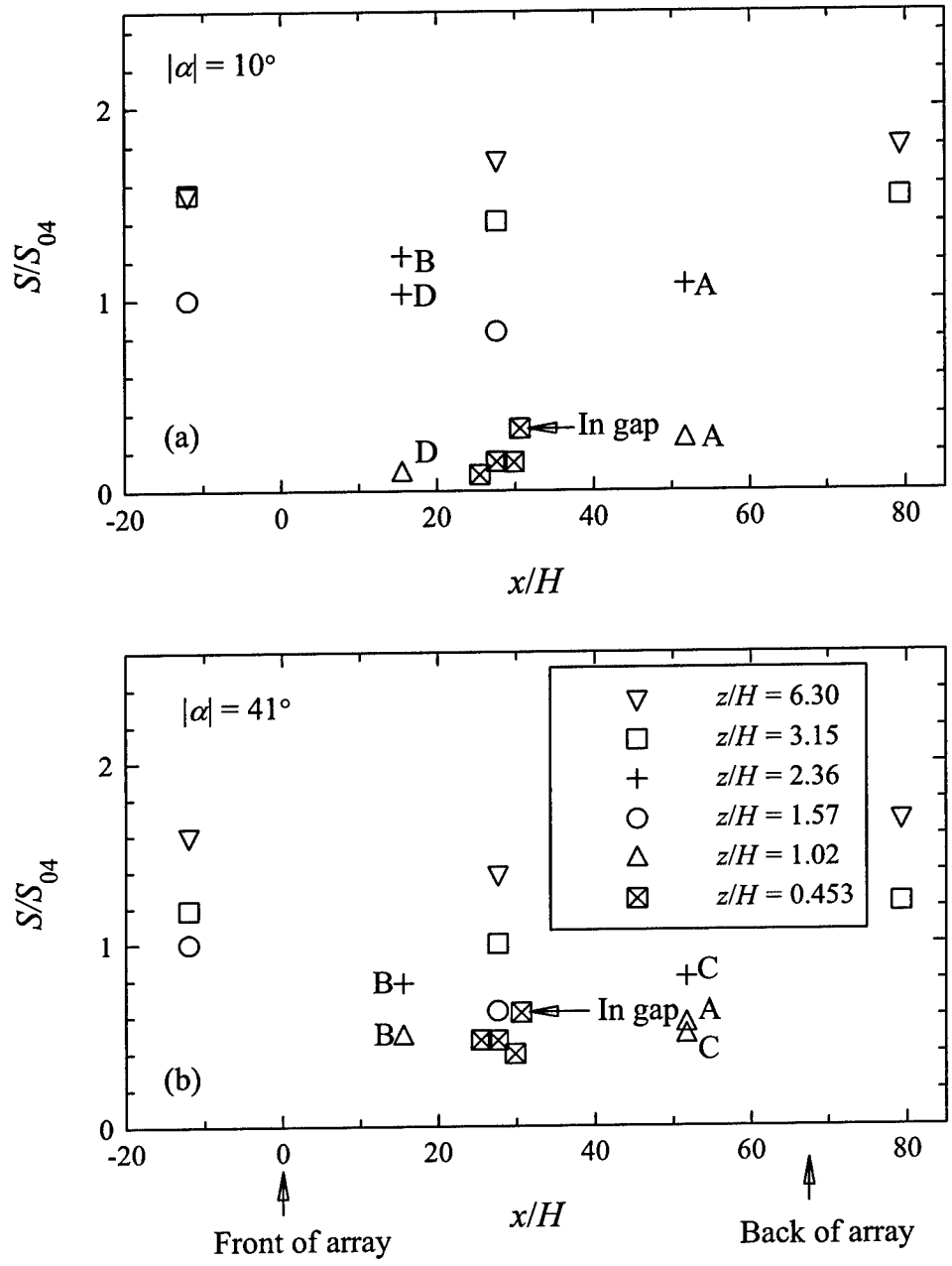

Figure 2. *Spatial variation of the normalized mean horizontal wind speed at various heights from the upwind fetch, through the obstacle array, and into the downwind fetch (a) for near perpendicular flow and (b) for a large obliquity of flow incidence. The letters A, B, C, or D associated with the data points indicate that the corresponding point was obtained from a sonic anemometer on towers A, B, C, or D, respectively (Figure 1). The label "in gap" refers to a measurement of the normalized mean horizontal wind speed made by the sonic anemometer (VX probe) positioned below the urban canopy height in the spanwise gap between obstacles G6 and G7.*

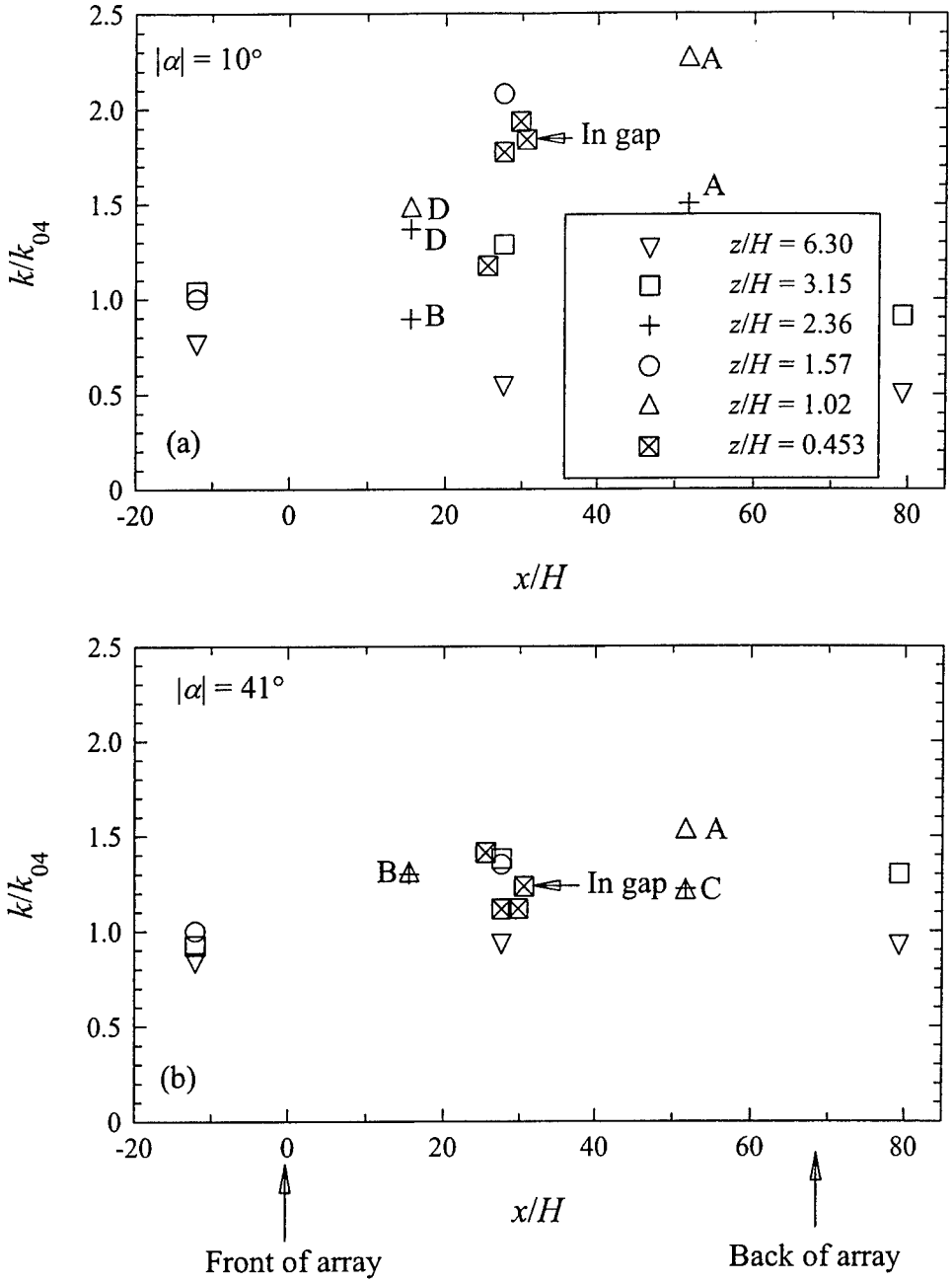

Figure 3. *Spatial variation of the normalized turbulence kinetic energy at various heights from the upwind fetch, through the obstacle array, and into the downwind fetch (a) for near perpendicular flow and (b) for a large flow incidence wind angle. The letters A, B, C, or D associated with the data points indicate that the corresponding point was obtained from a sonic anemometer on towers A, B, C, or D, respectively (Figure 1). The label "in gap" refers to a measurement of the normalized mean horizontal wind speed made by the sonic anemometer (VX probe) positioned below the urban canopy height in the spanwise gap between obstacles G6 and G7.*

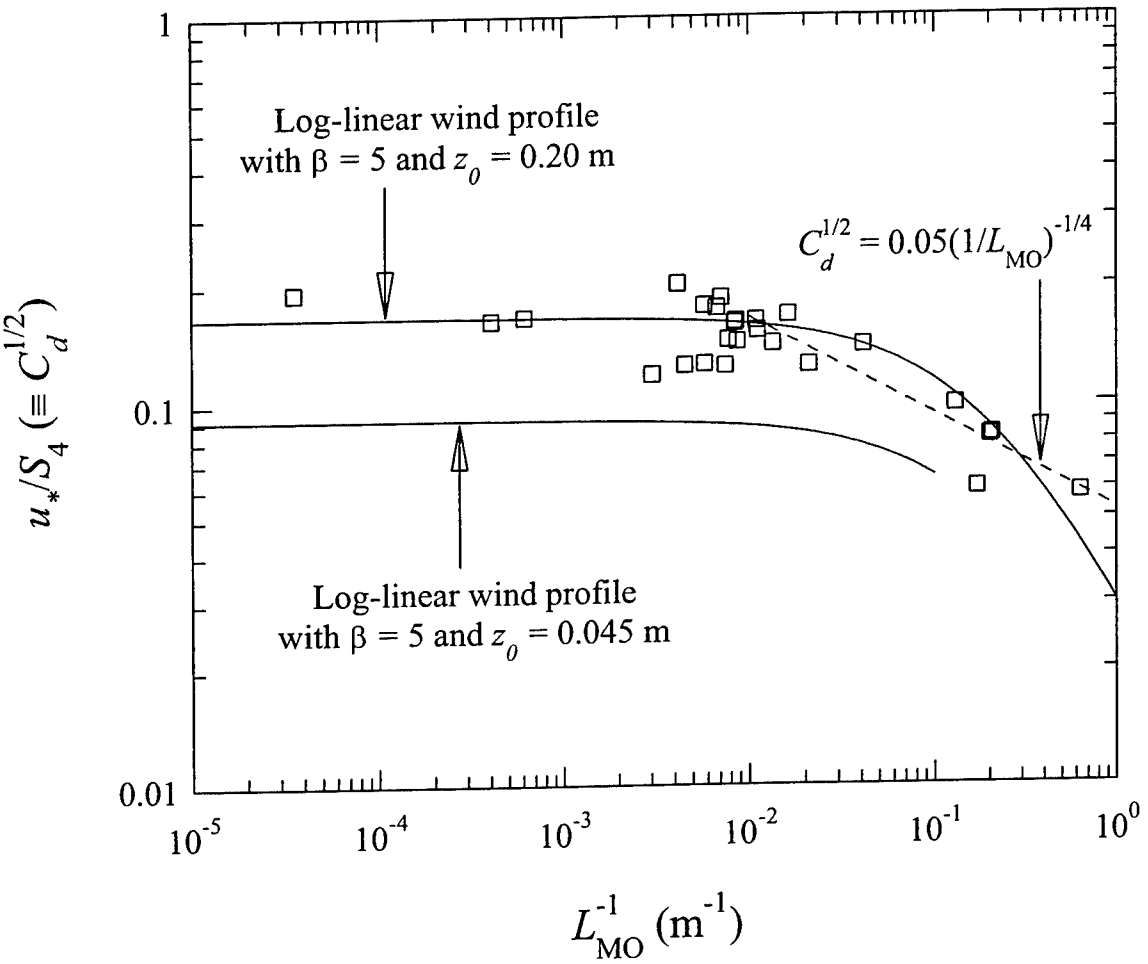

Figure 4. *Variation of the bulk drag coefficient with the stability parameter obtained from the 3-D sonic anemometer at the 4-m level on the 32-m vertical tower near the centre of the obstacle array.*

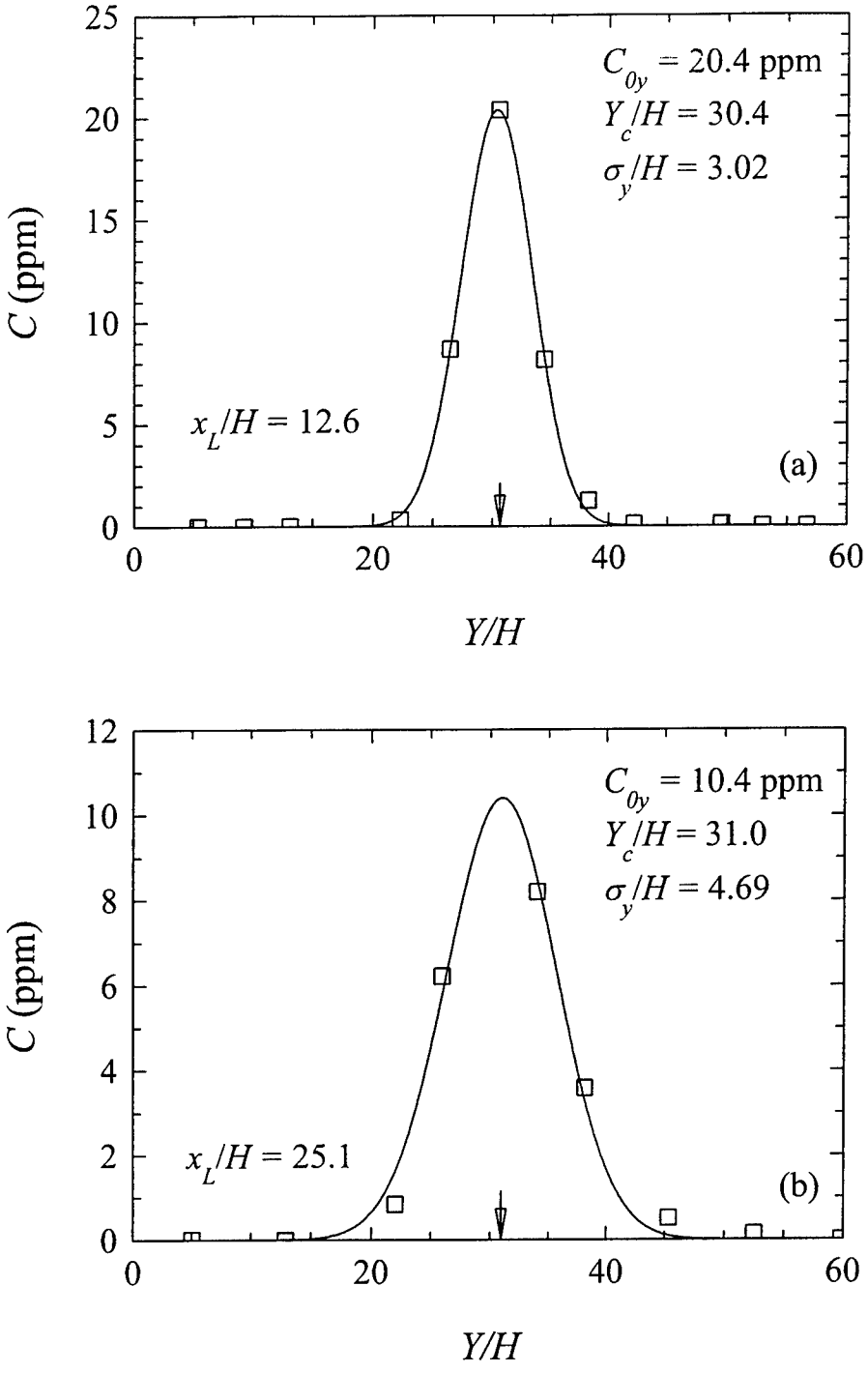

Figure 5. *Crosswind (lateral) mean concentration profiles measured at two normalized downwind distances from the source within the obstacle array for near perpendicular flow incidence. The data are extracted from two horizontal sampling lines in Trial 6. Superimposed on these profiles are the best-fit Gaussian distributions (see Eq. (6) for a definition of the fitted parameters). The arrows indicate the lateral position of the source.*

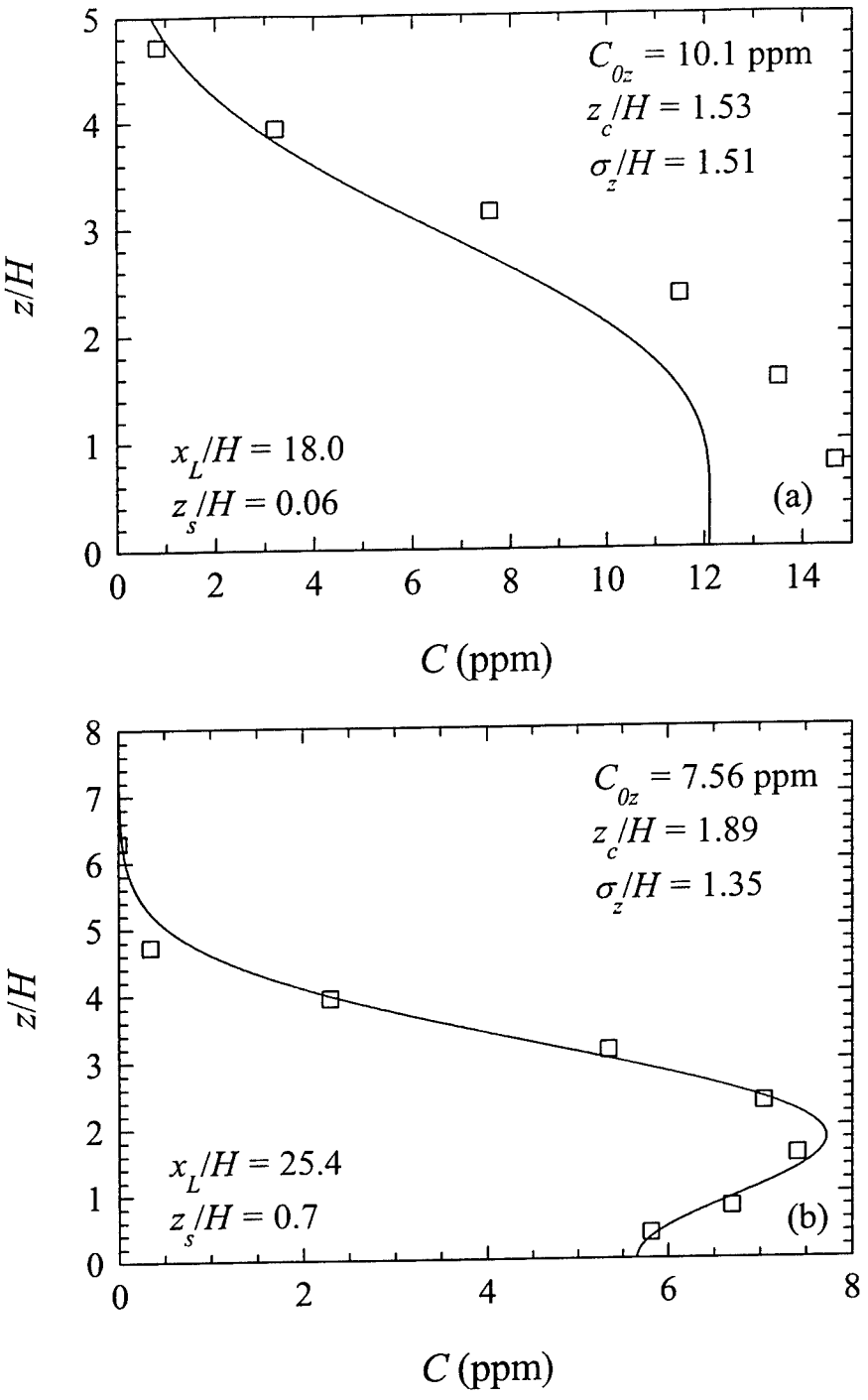

Figure 6. *Vertical profiles of the mean concentration at two normalized downwind distances and source release heights for array plumes. Figure 6(a) shows experiment number 6 at a normalized downwind distance of 18.0 with the source at a normalized height of 0.06, and Figure 6(b) shows experiment number 10 at a normalized downwind distance of 25.4 with the source at a normalized height of 0.7. Superimposed on these profiles are the best-fit reflected Gaussian distributions (see Eq. (7) for a definition of the fitted parameters).*

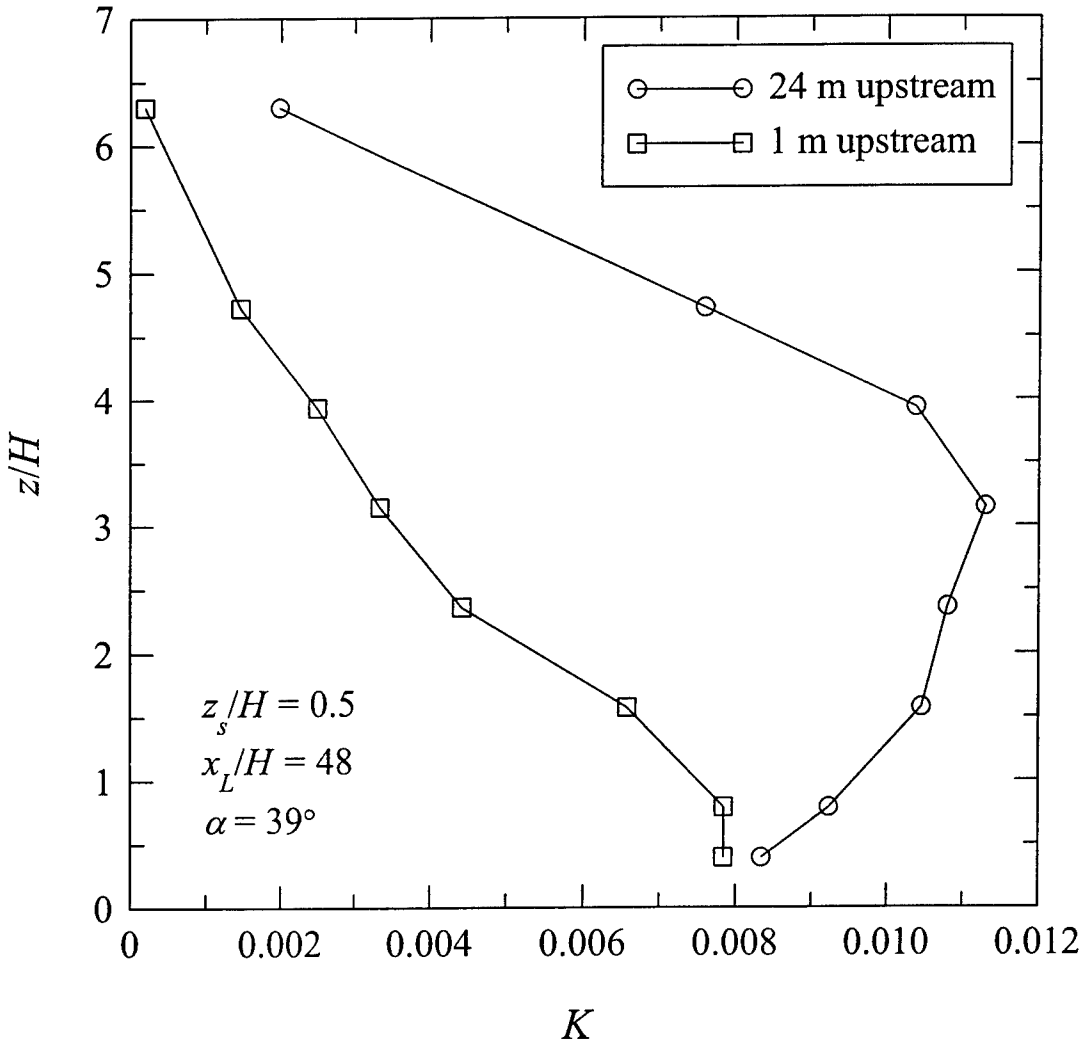

Figure 7. *Comparison of the vertical normalized mean concentration profiles along the plume centreline at a normalized downwind distance of 48.0 from the source for point sources location 1 m (Trial 18) and 24 m (Trial 17) upwind of the front face (at x= 0) of the obstacle array. For both releases, the incident wind direction was 39 degrees and the source was at a normalized height of 0.5.*

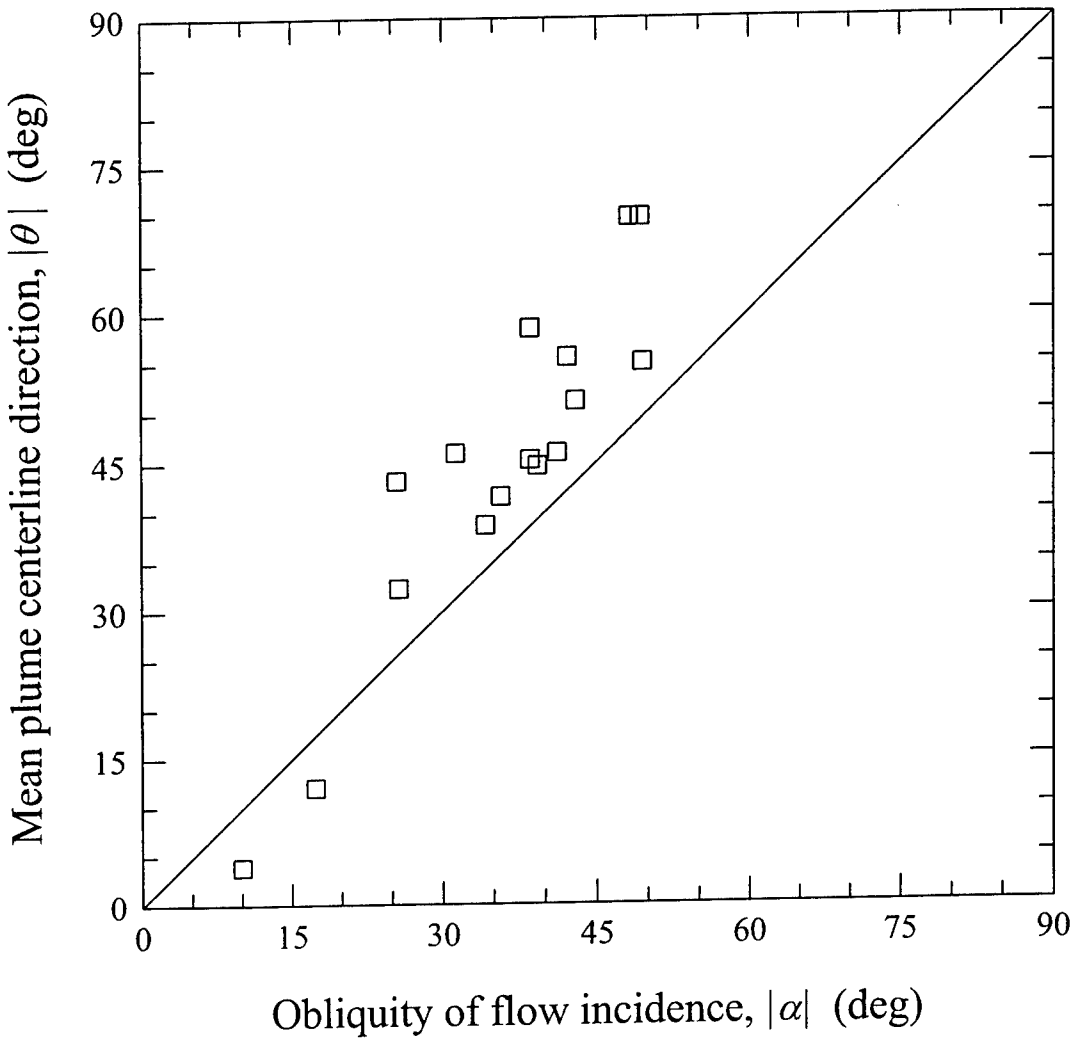

Figure 8. *The variation of the direction of the mean plume centreline with the obliquity of flow incidence.*

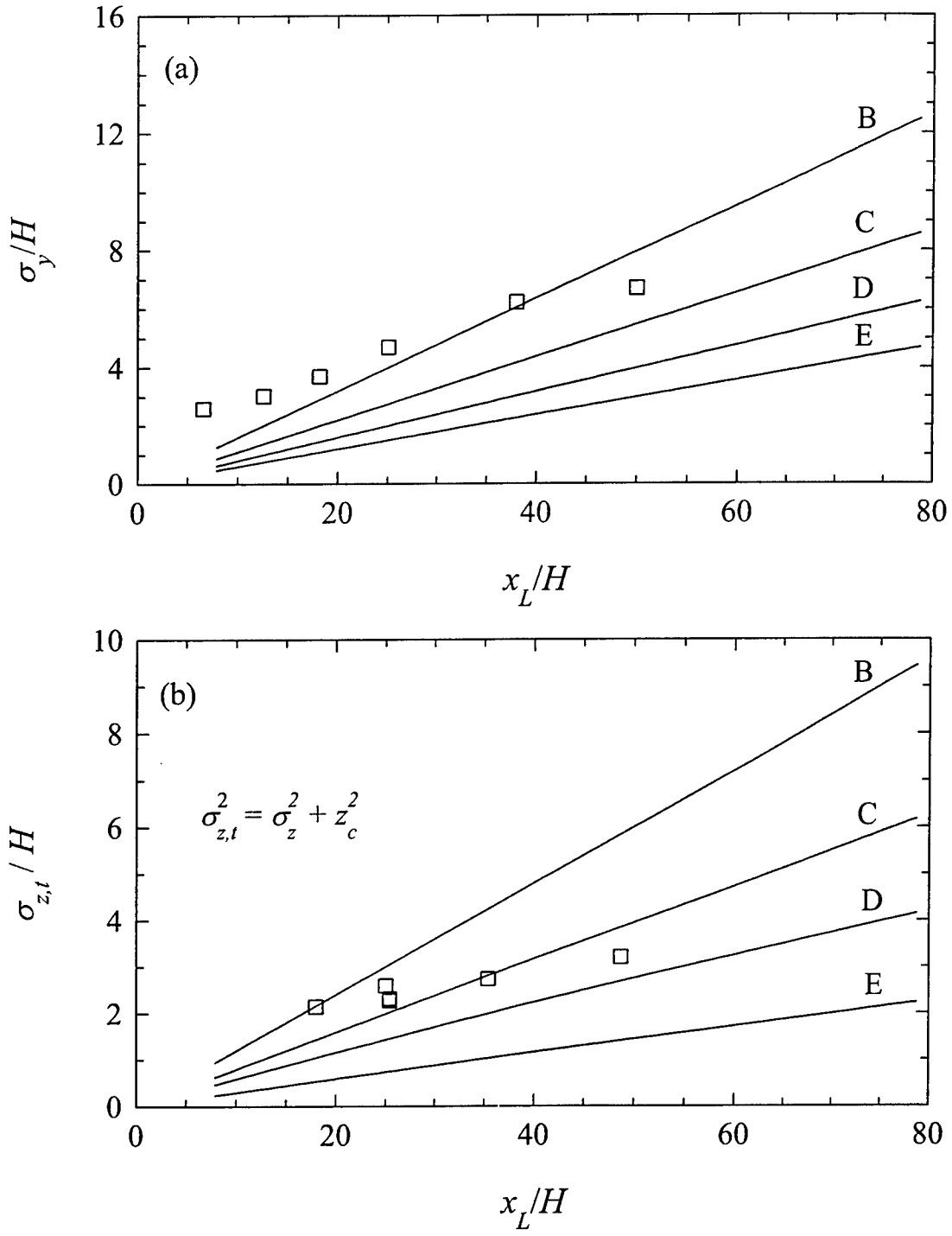

Figure 9. *The (a) lateral and (b) vertical growth of a plume dispersing in the obstacle array with nearly perpendicular flow incidence, compared with standard Pasquill-Gifford dispersion curves for open terrain for various atmospheric stability classes B, C, D, and E.*

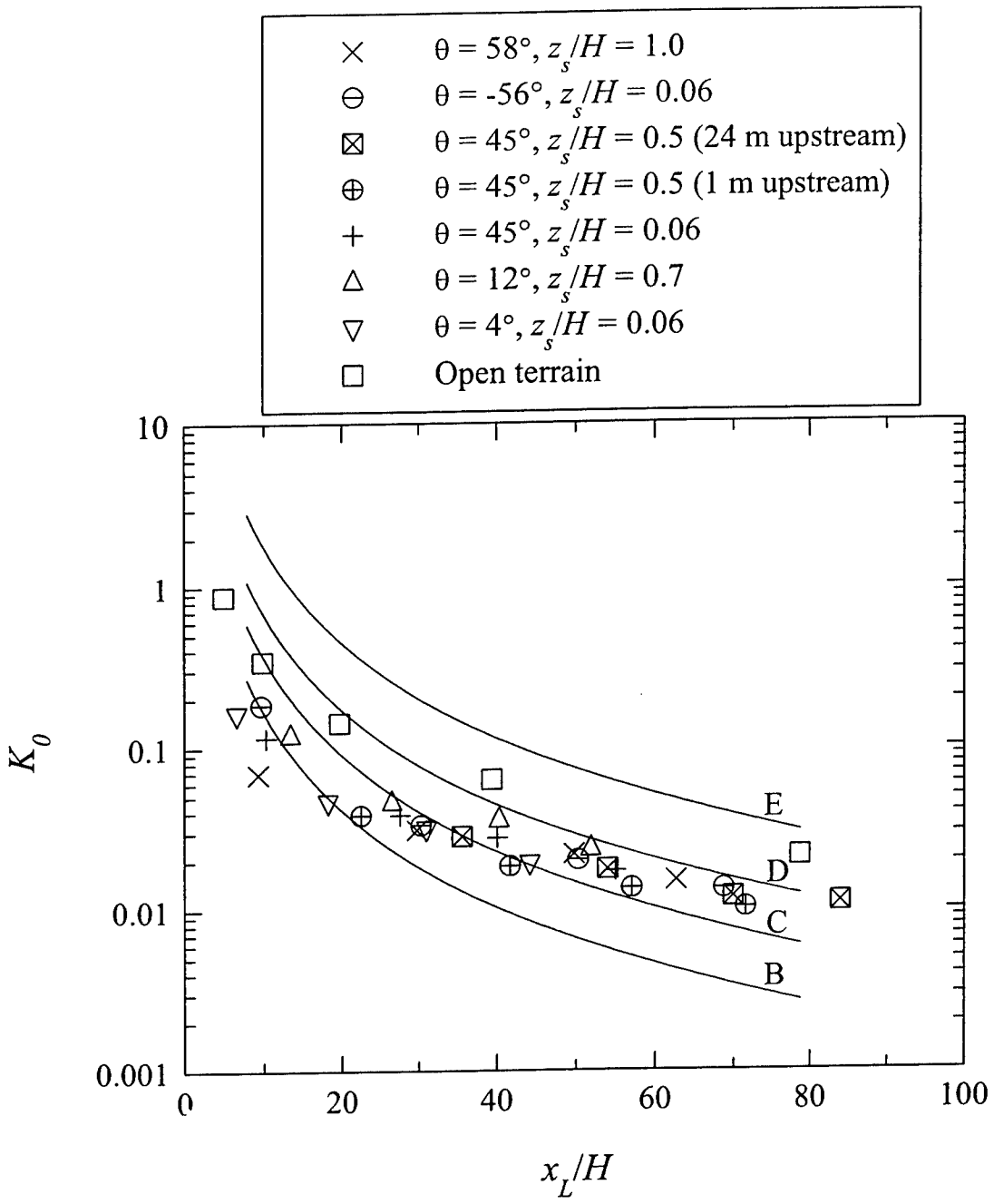

Figure 10. *The variation of the normalized mean plume centreline concentration with normalized downwind distance from the source through the obstacle array for various normalized source heights and directions of the plume centreline dispersion. The variation is compared with standard Gaussian plume model results using Pasquill-Gifford dispersion parameters for open (rural) terrain.*

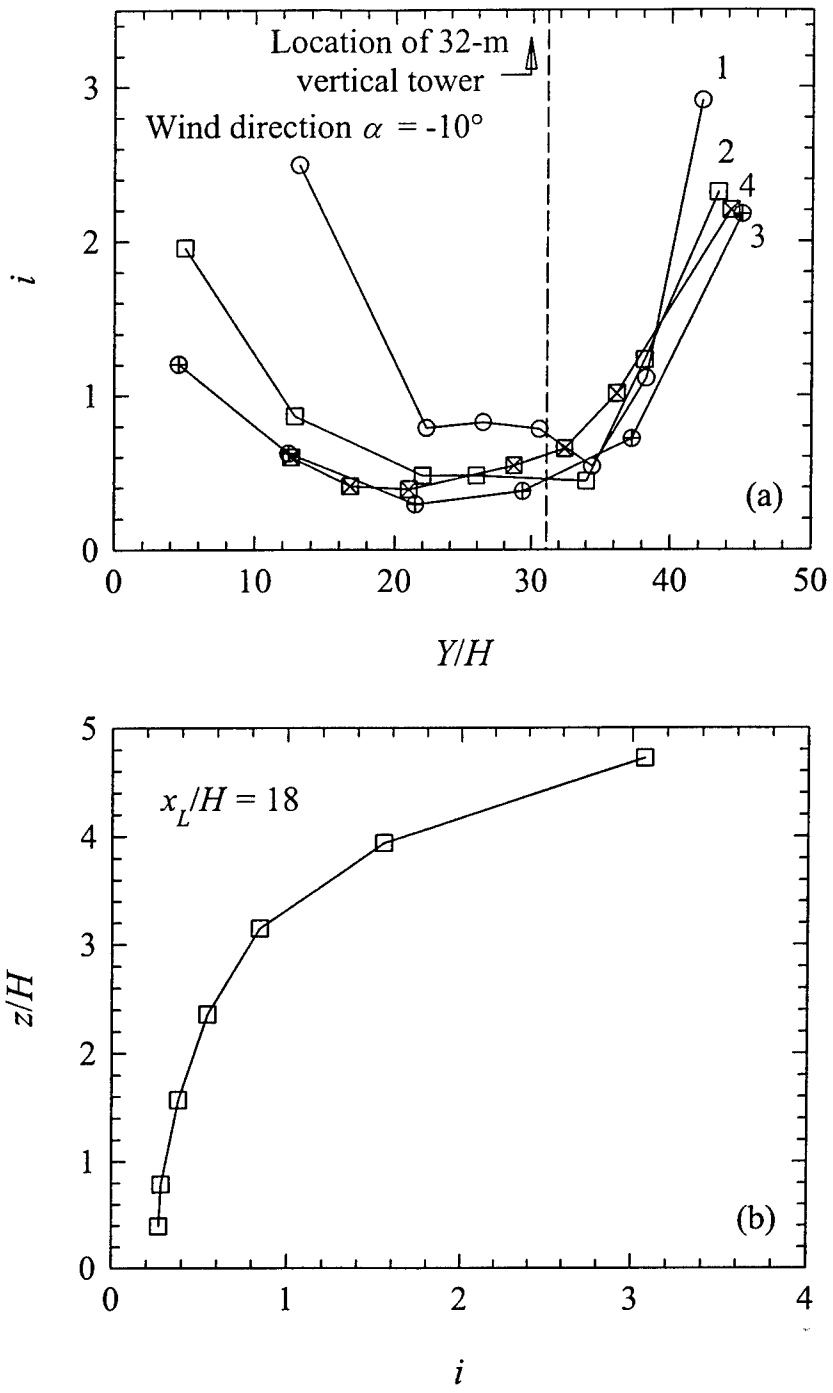

Figure 11. *(a) Crosswind cross-sections along four horizontal sampling lines (labeled 1, 2, 3, and 4) at various normalized downwind distances from the source and (b) a vertical profile obtained on the 32-m vertical tower of the fluctuation intensity in an array plume with near perpendicular flow incidence. Crosswind profiles of fluctuation intensity were measured at normalized downwind distances from the source of 6.6, 18, 31, and 42. The dashed line indicates the lateral position of the source. The data for this example were extracted from Trial 6.*

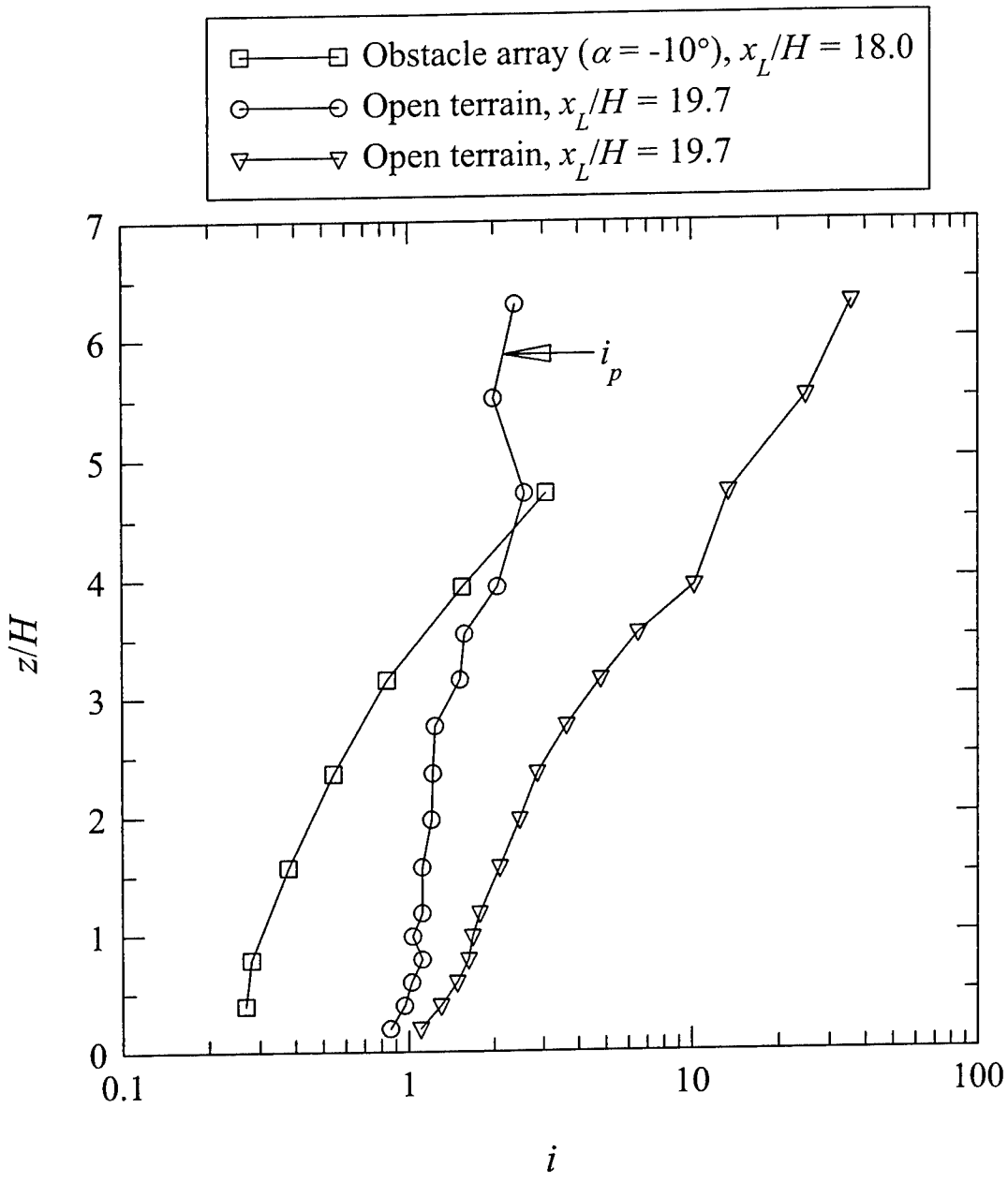

Figure 12. *Comparisons of vertical profiles of fluctuation intensity measured in the array plume with those measured in an open-terrain plume under similar atmospheric conditions and at about the same downwind distance from the source. The vertical profile of the conditional fluctuation intensity in the open-terrain plume is also shown for comparison.*

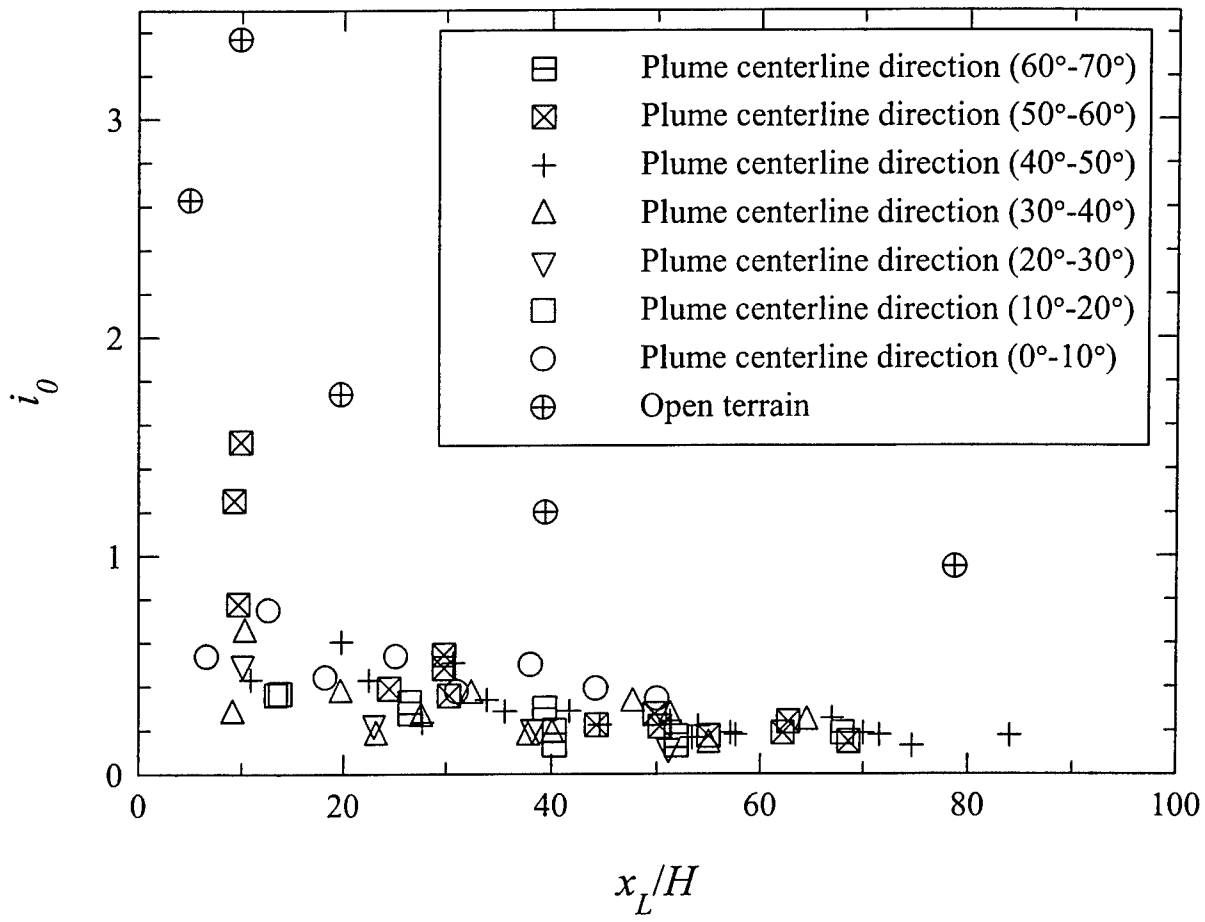

Figure 13. *Plume centreline values of fluctuation intensity plotted against normalized downwind distance from the source for dispersion over open terrain and inside the obstacle array for various directions of plume centreline dispersion.*

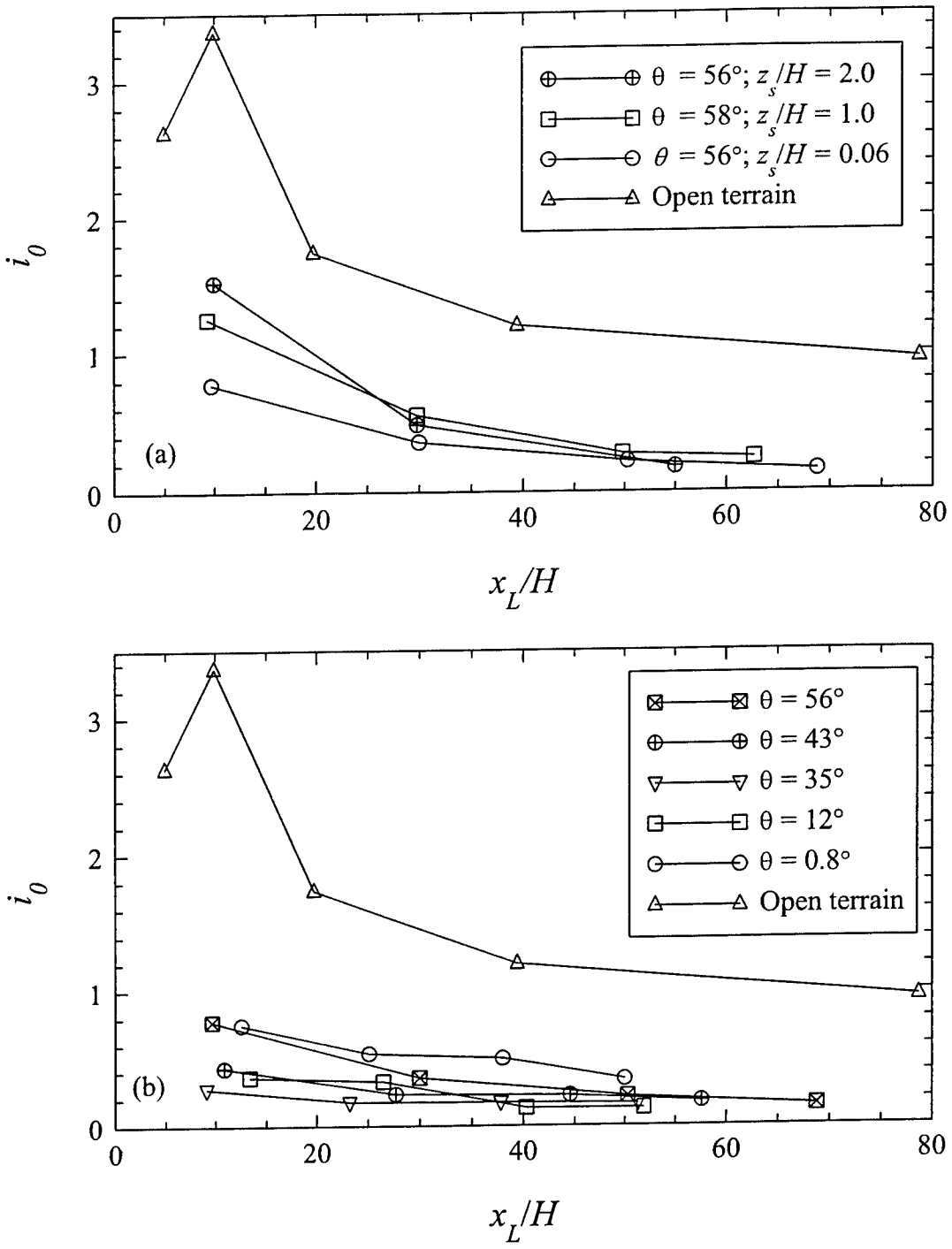

Figure 14. *Decay of plume centreline fluctuation intensity with normalized downwind distance from the source stratified according to (a) source release height at a fixed direction of plume centreline dispersion and (b) by the direction of plume centreline dispersion through the obstacle array.*

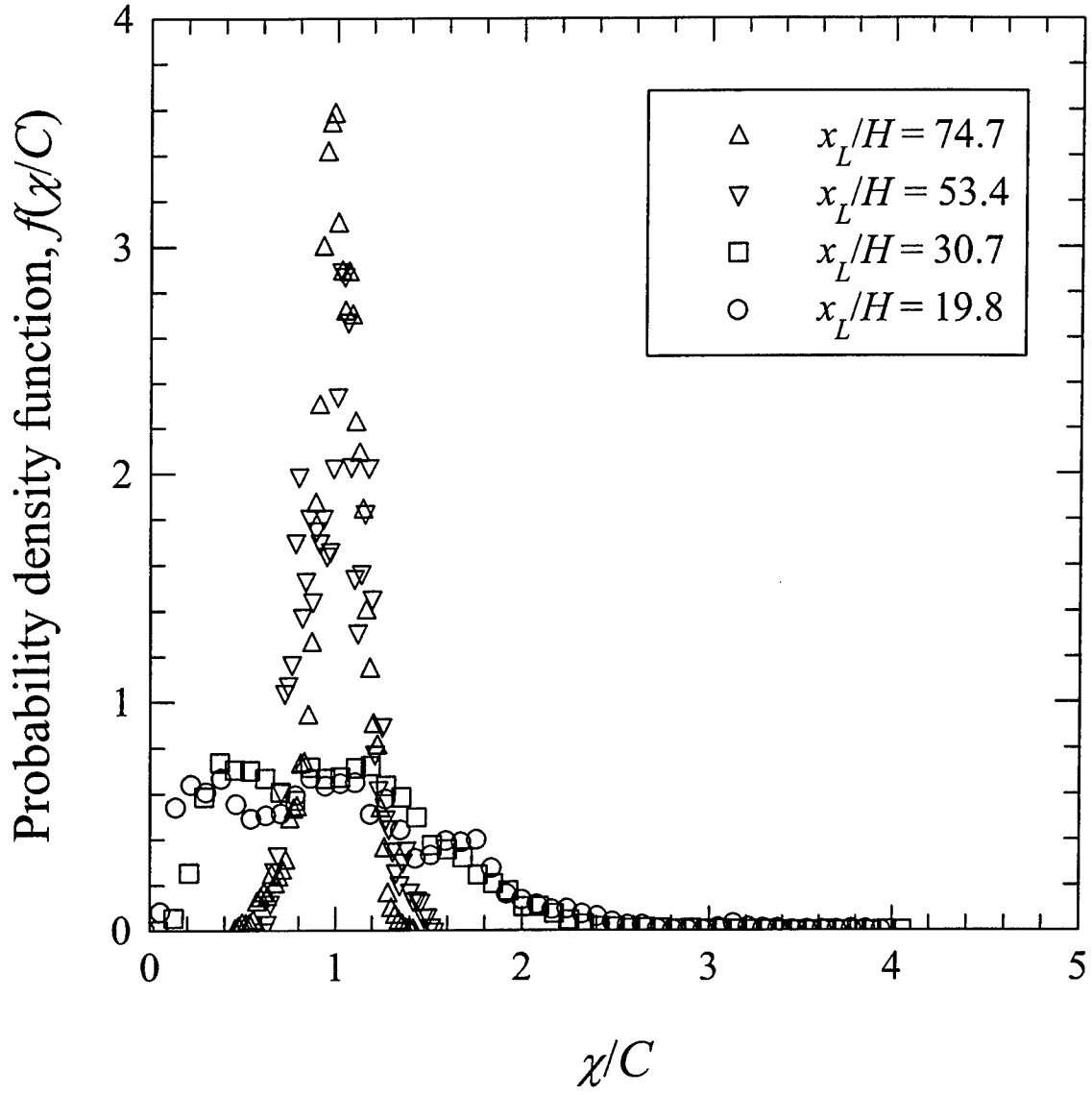

Figure 15. *Probability density function of normalized concentration measured along the centreline of a dispersing plume within the array at a fixed normalized height of 0.71 at various non-dimensional downwind distances from the source. The data for this example were extracted from Trial 13.*

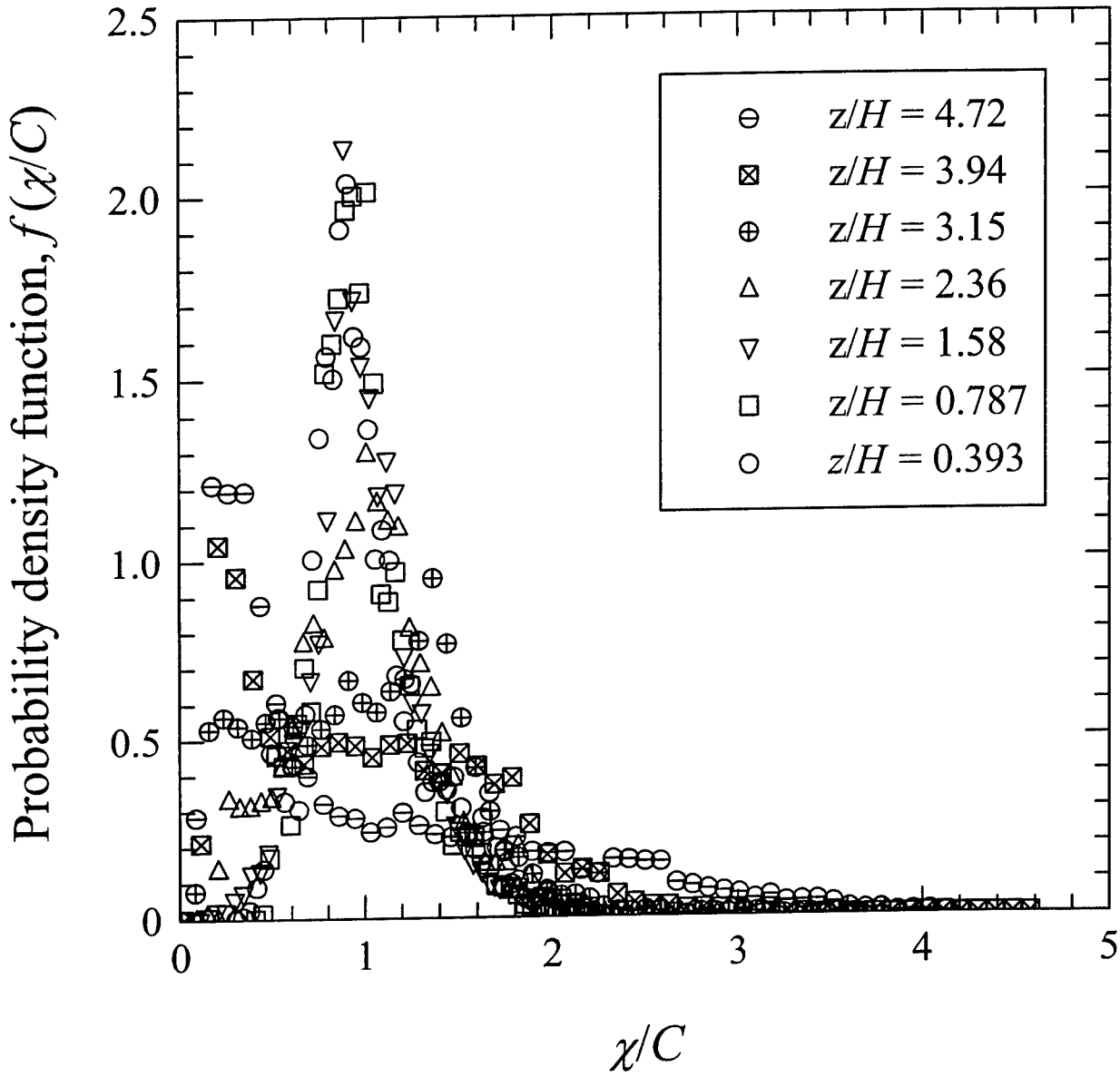

Figure 16. *Vertical profiles of the probability density function of normalized concentration measured along the centreline of a dispersing plume within the array at a fixed non-dimensional downwind distance of 30.7 from the source. The data for this example was taken from Trial 13.*

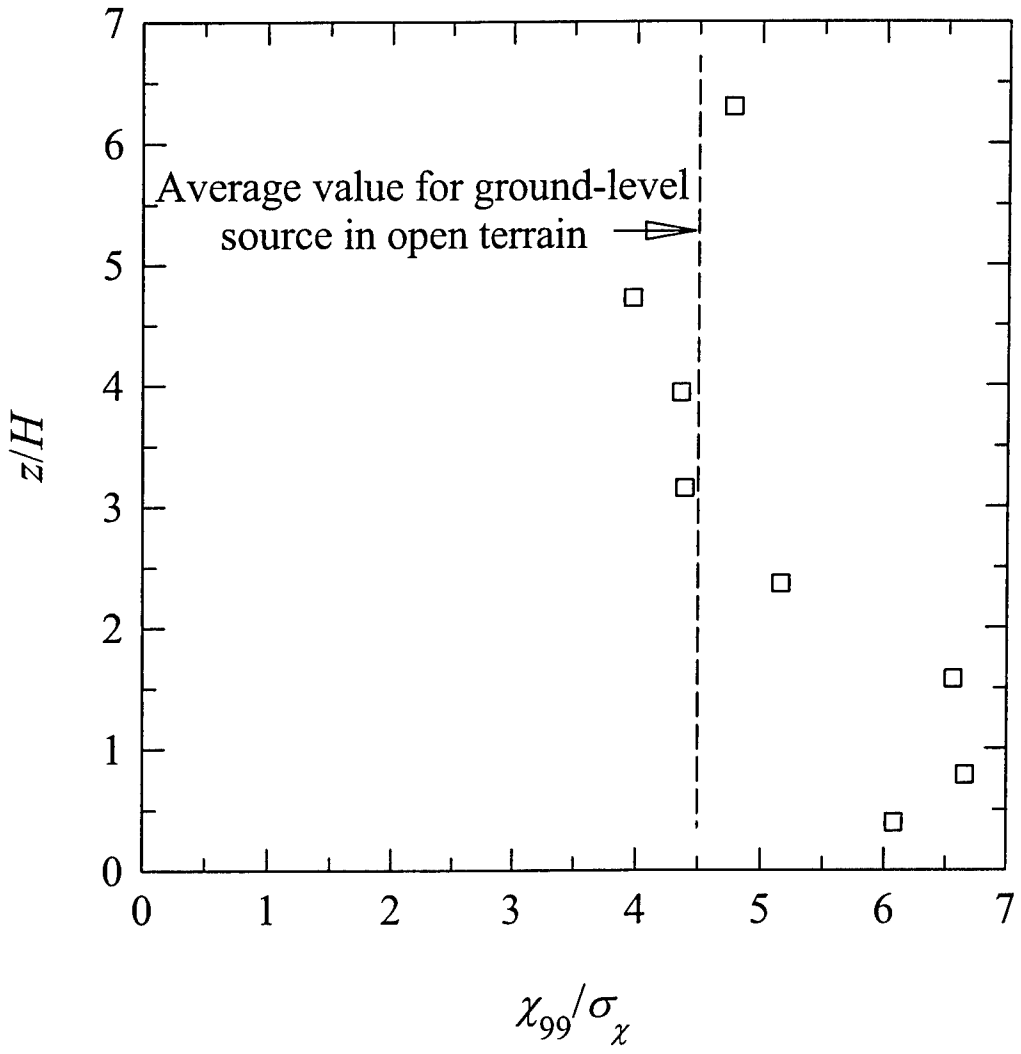

Figure 17. *Vertical profiles of the ratio of the peak concentration to the concentration standard deviation measured along the centreline of an array plume at a normalized downwind distance from the source of 30.7. The data for this example were extracted from Trial 13.*

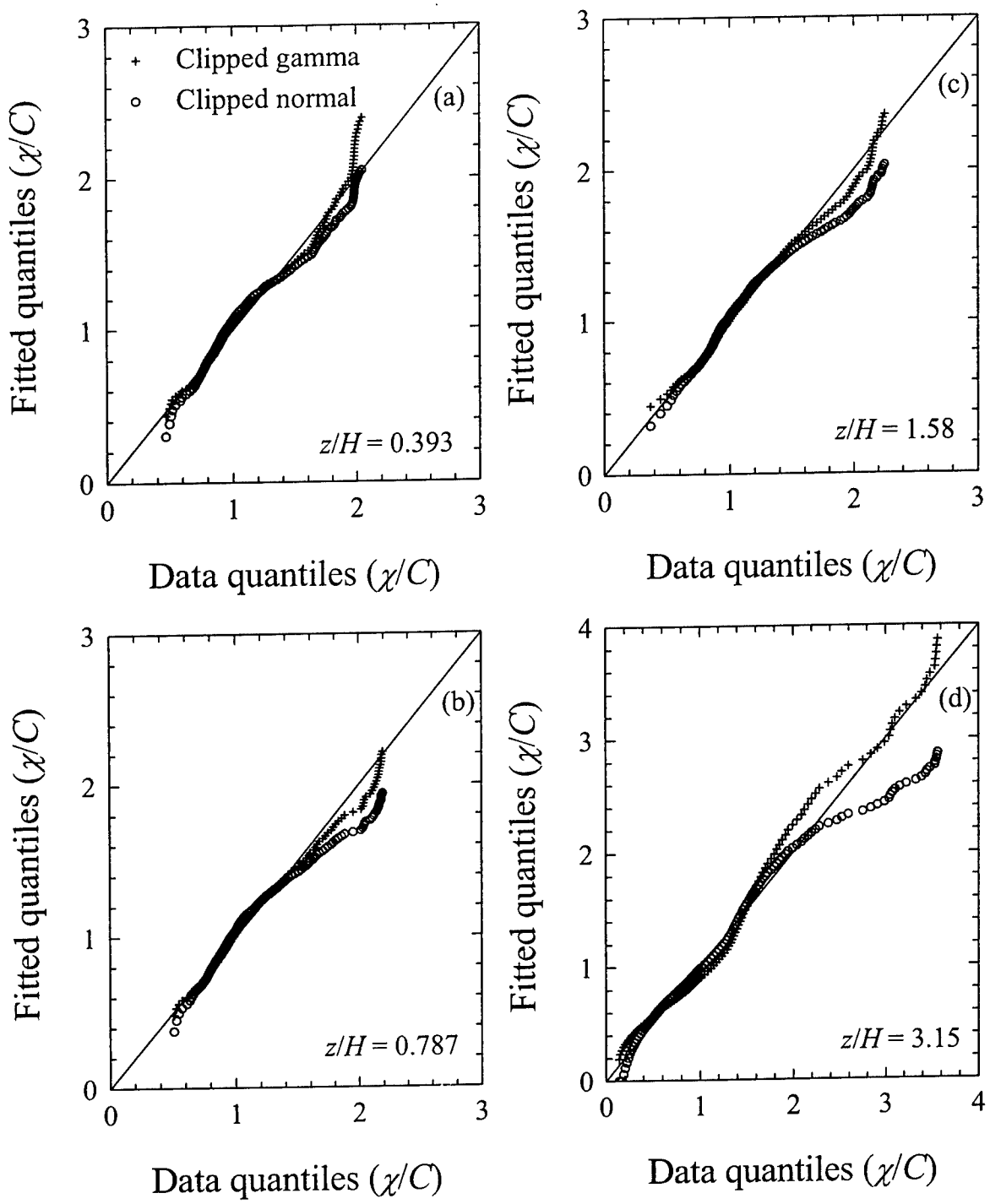

Figure 18. *Quantile-quantile (Q-Q) plots comparing the normalized concentration data quantiles with the associated model quantiles of the fitted clipped normal and clipped gamma distributions. The data were extracted from Trial 13 at various heights in the plume at a non-dimensional downwind distance from the source of 30.7.*

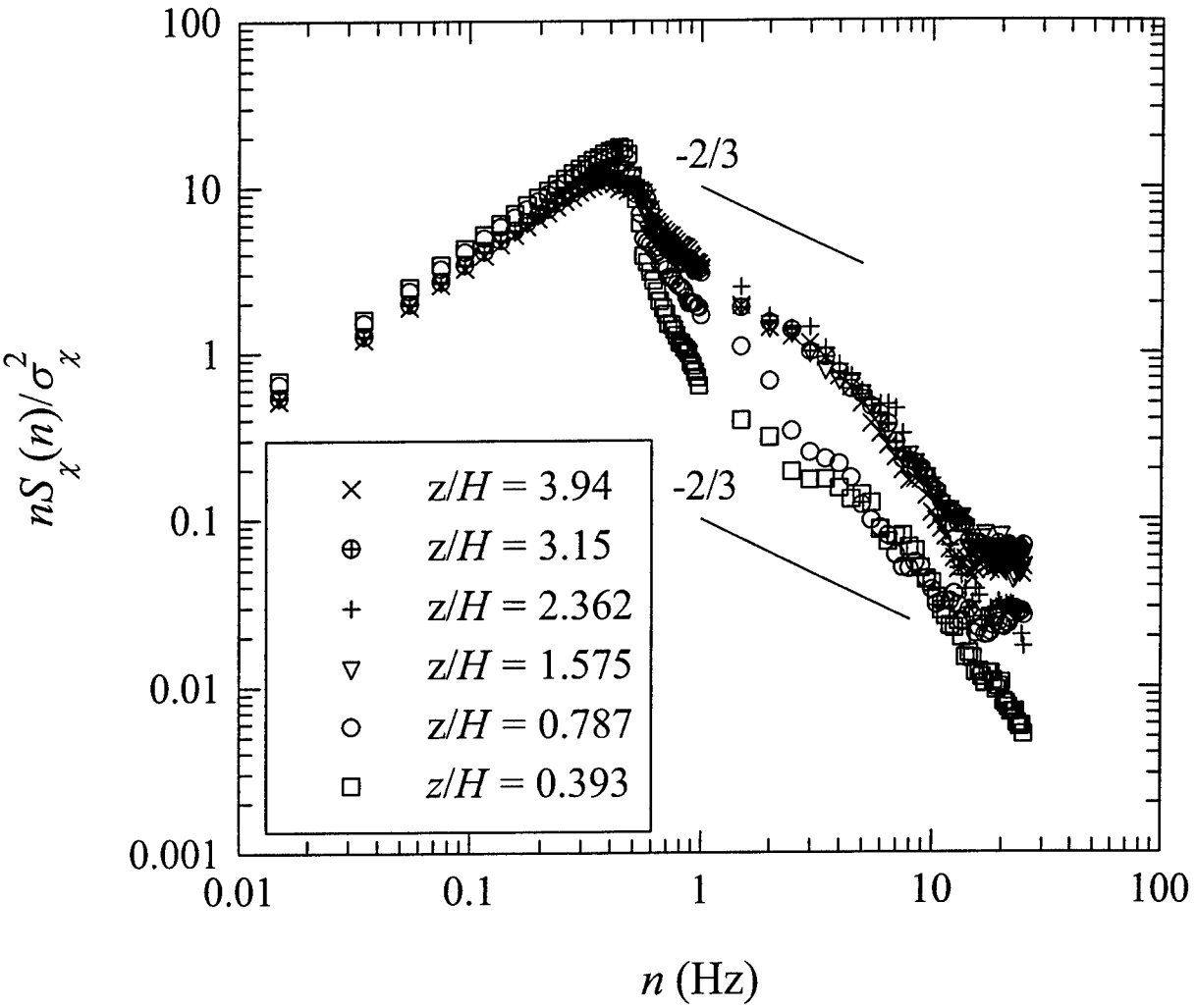

Figure 19. *Vertical variation of the normalized power spectrum of concentration fluctuations. A straight line with a slope of -2/3 has been included in the logarithmic plots for comparison with the spectra. The data were extracted from Trial 13 at various heights in the plume at a non-dimensional downwind distance from the source of 30.7.*

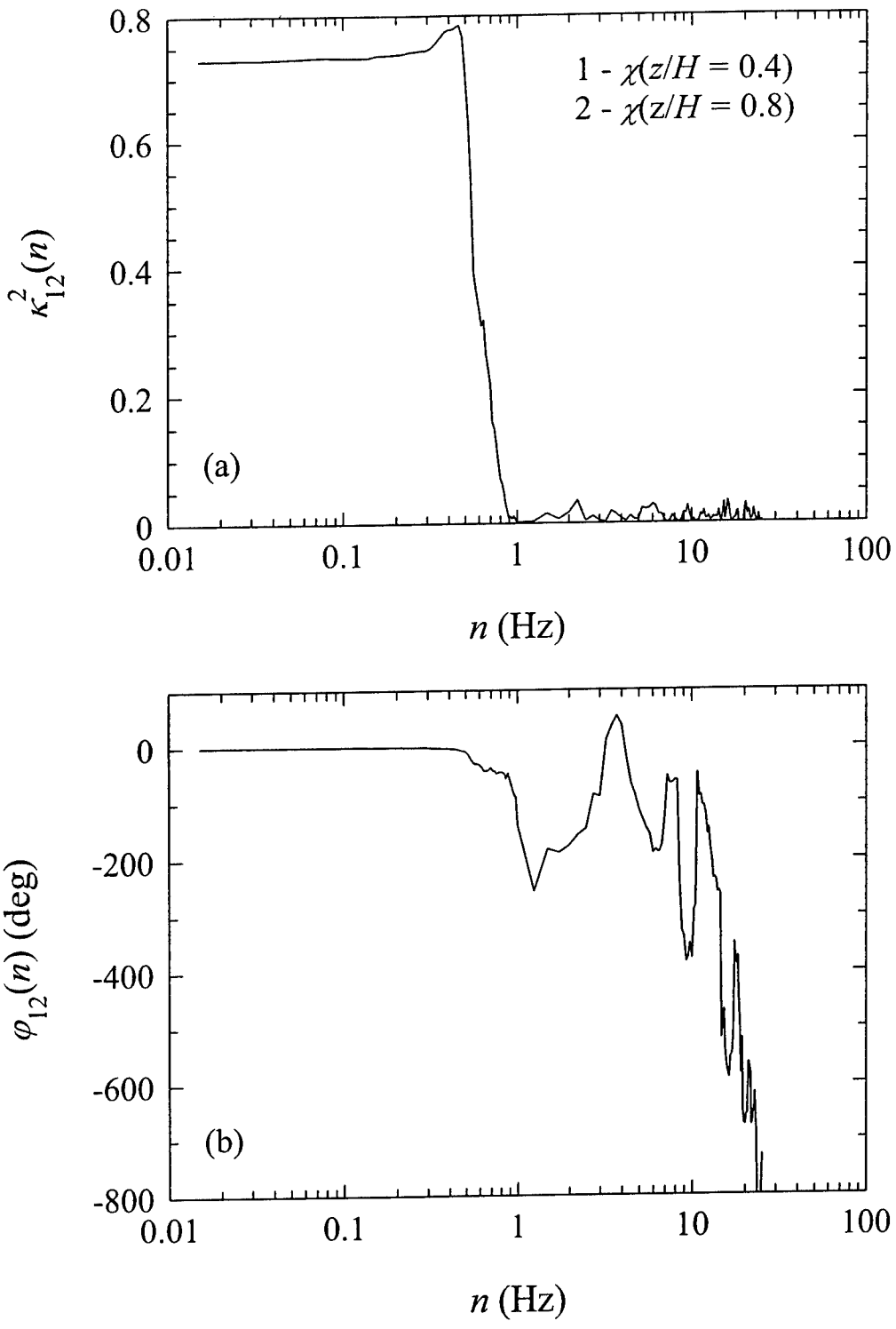

Figure 20. *(a) Squared coherency and (b) phase spectra between two concentration time series measured at two different heights below the top of the obstacle array. The data for this example were extracted from Trial 13.*

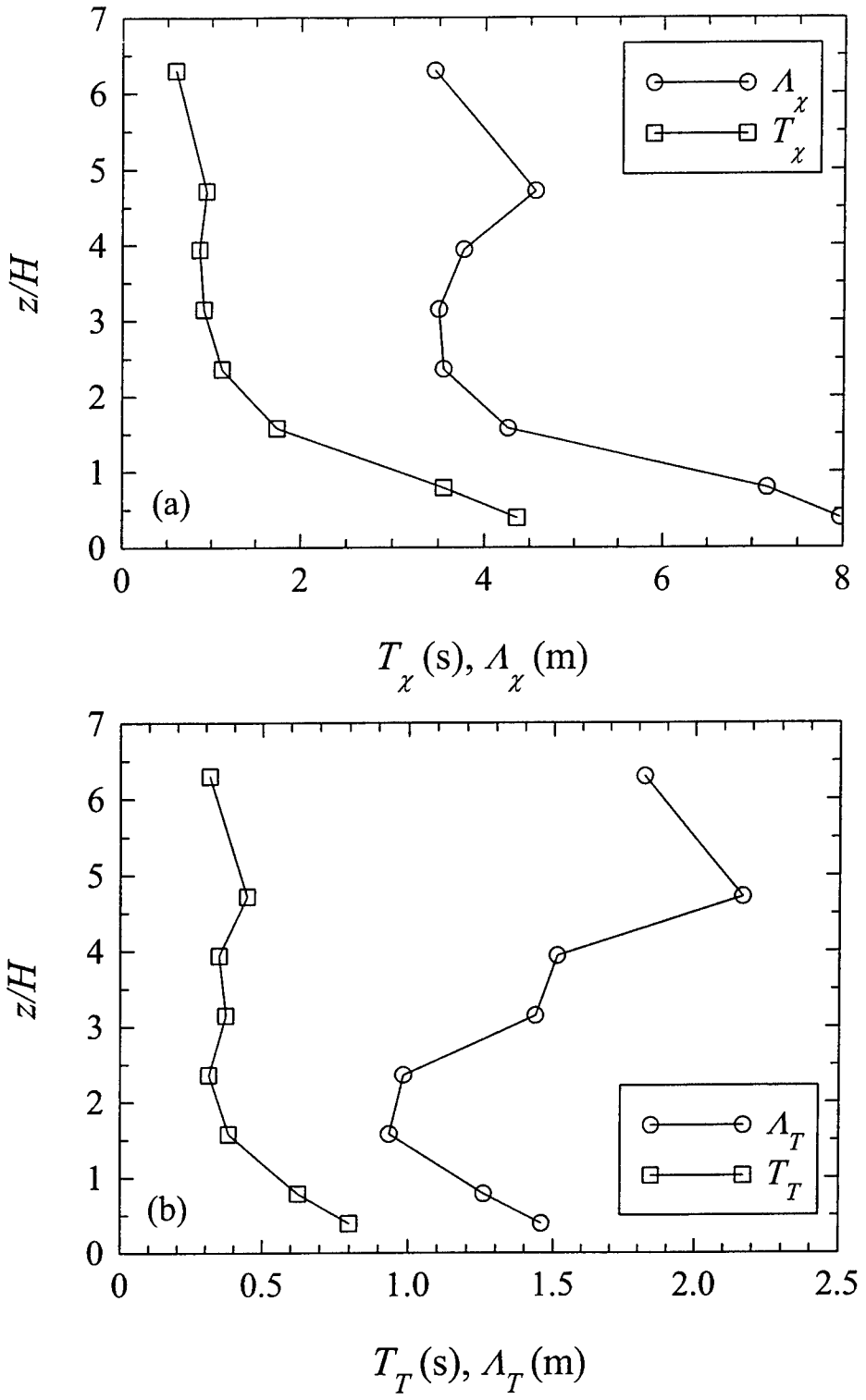

Figure 21. *Vertical profiles of (a) concentration integral time and length scales and (b) Taylor microscale time and length scales measured in the array plume along the mean plume centreline at a normalized downwind distance from the source of 30.7. The data for this example were extracted from Trial 13.*

UNCLASSIFIED

SECURITY CLASSIFICATION OF FORM

(highest classification of Title, Abstract, Keywords)

DOCUMENT CONTROL DATA

(Security classification of title, body of abstract and indexing annotation must be entered when the overall document is classified)

1. ORIGINATOR (the name and address of the organization preparing the document. Organizations for who the document was prepared, e.g. Establishment sponsoring a contractor's report, or tasking agency, are entered in Section 8.)

   Defence R&D Canada – Suffield

2. SECURITY CLASSIFICATION (overall security classification of the document, including special warning terms if applicable)

   Unclassified

3. TITLE (the complete document title as indicated on the title page. Its classification should be indicated by the appropriate abbreviation (S, C or U) in parentheses after the title).

   Mock Urban Setting Trail: Data Analysis and Interpretation (U)

4. AUTHORS (Last name, first name, middle initial. If military, show rank, e.g. Doe, Maj. John E.)

   Yee, Eugene

5. DATE OF PUBLICATION (month and year of publication of document)

   December 2003

6a. NO. OF PAGES (total containing information, include Annexes, Appendices, etc) 83

6b. NO. OF REFS (total cited in document) 39

7. DESCRIPTIVE NOTES (the category of the document, e.g. technical report, technical note or memorandum. If appropriate, enter the type of report, e.g. interim, progress, summary, annual or final. Give the inclusive dates when a specific reporting period is covered.)

   Technical Report (Final) September 2001 – April 2003

8. SPONSORING ACTIVITY (the name of the department project office or laboratory sponsoring the research and development. Include the address.)

   DRDC Suffield

9a. PROJECT OR GRANT NO. (If appropriate, the applicable research and development project or grant number under which the document was written. Please specify whether project or grant.)

   PCN 16QD11

9b. CONTRACT NO. (If appropriate, the applicable number under which the document was written.)

10a. ORIGINATOR'S DOCUMENT NUMBER (the official document number by which the document is identified by the originating activity. This number must be unique to this document.)

   DRDC Suffield TR 2003-097

10b. OTHER DOCUMENT NOs. (Any other numbers which may be assigned this document either by the originator or by the sponsor.)

11. DOCUMENT AVAILABILITY (any limitations on further dissemination of the document, other than those imposed by security classification)

   (x) Unlimited distribution
   ( ) Distribution limited to defence departments and defence contractors; further distribution only as approved
   ( ) Distribution limited to defence departments and Canadian defence contractors; further distribution only as approved
   ( ) Distribution limited to government departments and agencies; further distribution only as approved
   ( ) Distribution limited to defence departments; further distribution only as approved
   ( ) Other (please specify):

12. DOCUMENT ANNOUNCEMENT (any limitation to the bibliographic announcement of this document. This will normally corresponded to the Document Availability (11). However, where further distribution (beyond the audience specified in 11) is possible, a wider announcement audience may be selected). NONE

13. ABSTRACT (a brief and factual summary of the document. It may also appear elsewhere in the body of the document itself. It is highly desirable that the abstract of classified documents be unclassified. Each paragraph of the abstract shall begin with an indication of the security classification of the information in the paragraph (unless the document itself is unclassified) represented as (S), (C) or (U). It is not necessary to include here abstracts in both official languages unless the text is bilingual).

(U) This report describes a comprehensive study of the statistical characteristics of concentration fluctuations in a neutrally buoyant tracer plume dispersing through a large array of building-like obstacles, each of which measured 12.2 m × 2.42 m × 2.54 m. The plumes were released both upwind and within the obstacle array for a range of source heights between 0.15 and 5.2 m. Detailed flow field and instantaneous plume concentration data were obtained from a comprehensive series of tracer experiments which utilized a large number of high-resolution concentration detectors, accompanied by the simultaneous acquisition of meteorological and turbulence measurements with sonic anemometer/thermometers. Extensive analyses are performed on the plume concentration data, and results are presented for a number of concentration statistics such as the mean plume lateral and vertical spreads, mean concentration, fluctuation intensity, peak concentration to concentration standard deviation ratio, concentration probability density function (pdf), concentration power spectra, and various concentration time and length scales of dominant motions in the array plume (e.g., integral scale, Taylor microscale).

(U) For the range of downwind distances from the source examined, the lateral mean concentration profiles are well approximated by a Gaussian distribution. The vertical profiles of mean concentration develop in a rather complex manner with downwind distance, with the result that the reflected Gaussian form is generally a less than ideal description of the mean array plume in the vertical direction. A comparison of the array plume with an open-terrain plume as a function of downwind distance indicates that the obstacle array significantly increases the lateral and vertical plume spreads and decreases the magnitude of the plume centreline mean concentration. The small-scale, high-intensity turbulence generated in the obstacle array results in a drastic reduction in the concentration fluctuation level in the array plume compared to an open-terrain plume under similar conditions. The evolution of the concentration pdf at a fixed range, but with decreasing height from above and into the obstacle array is similar to that obtained at a fixed height but with increasing downwind distance from the source. The integral and Taylor microscale time and length scales of the plume increase significantly within the obstacle array. Concentration power spectra measured within the array had a greater proportion of the total concentration variance in the lower frequencies (energetic subrange), with a correspondingly smaller proportion in the higher frequencies (inertial-convective subrange). It is believed that these effects result from the rapid and efficient stirring and mixing of plume material by the small-scale, high-intensity turbulence within the array.

14. KEYWORDS, DESCRIPTORS or IDENTIFIERS (technically meaningful terms or short phrases that characterize a document and could be helpful in cataloguing the document. They should be selected so that no security classification is required. Identifies, such as equipment model designation, trade name, military project code name, geographic location may also be included. If possible keywords should be selected from a published thesaurus, e.g. Thesaurus of Engineering and Scientific Terms (TEST) and that thesaurus-identified. If it is not possible to select indexing terms which are Unclassified, the classification of each should be indicated as with the title.)

Atmospheric dispersion
Obstacle Array
Urban Flow
Urban Dispersion
Fast-response concentration detectors